INSTITUTO
UNIVERSITÁRIO
DE LISBOA

Capacity Limits of Crosstalk-limited Multi-core Fiber Systems

Ana Margarida Filipe Domingues

Master in Telecommunications and Computer Engineering

Supervisor:
Prof. Dr. Adolfo Cartaxo, Full Professor
ISCTE-IUL

Co-Supervisor:
Prof. Dr. João Rebola, Assistant Professor
ISCTE-IUL

September, 2020

TECNOLOGIAS
E ARQUITETURA

Capacity Limits of Crosstalk-limited Multi-core Fiber Systems

Ana Margarida Filipe Domingues

Master in Telecommunications and Computer Engineering

Supervisor:
Prof. Dr. Adolfo Cartaxo, Full Professor
ISCTE-IUL

Co-Supervisor:
Prof. Dr. João Rebola, Assistant Professor
ISCTE-IUL

September, 2020

Acknowledgements

Firstly, I would like to express my gratitude to my supervisors, Professor Adolfo Cartaxo and Professor João Rebola, for their availability, support, motivation and knowledge that were crucial to the elaboration of this work. I want to acknowledge Instituto de Telecomunicações (IT)-IUL and Iscte-Instituto Universitário de Lisboa, for providing the means to enable me to carry out this work.

Secondly, I would also thank my family for all their unconditional support.

Finally, I want to thank my boyfriend, Simão, for his motivation and support.

Resumo

A multiplexagem por divisão no espaço usando fibras ópticas multi-núcleo tem sido extensivamente proposta para conseguir transmissão de capacidade ultra-elevada e lidar com o facto de que fibra composta por um núcleo estar perto de atingir o seu limite. Já foram demonstradas transmissões com capacidades na ordem dos petabit por segundo usando fibras multi-núcleo. O desempenho destes sistemas, é, no limite, imposto pela diafonia entre núcleos e por isso é feita uma análise da diafonia em sistemas coerentes que utilizam a grelha flexível na banda C. A capacidade do sistema é dada pelo número de núcleos permitidos nas fibras multi-núcleo fracamente acopladas para cada formato de modulação que é imposta pela potência média máxima da diafonia entre núcleos para uma dada distância. Os constrangimentos da ligação, como a dependência do comprimento de onda da potência da diafonia entre núcleos na banda de transmissão e o efeito da interferência não linear, são considerados. A capacidade de redes metropolitanas, regionais e de longa distância são avaliadas para as fibras multi-núcleo de perfil fracamente acopladas. Considerando os constrangimentos da ligação como a dependência do comprimento de onda da potência da diafonia entre núcleos na banda de transmissão e os efeitos não lineares, a capacidade total de 483.84 Tb/s usando o formato de modulação 32-QAM , 430 Tb/s usando o formato de modulação 32-QAM e 206.08 Tbs/s e usando o formato de modulação 4-QAM é alcançada para as redes metropolitanas (50 km), regionais (500 km) e de longa distância (5000 km), respectivamente.

Palavras-chave: Diafonia, Fibras multi-núcleo, Formatos de modulação, Multiplexagem por divisão no espaço, Redes ópticas.

Abstract

Space division multiplexing (SDM) is mainly seen as a way to increase data throughput and handle the fact that the data capacity of single mode single core fiber (SM-SCF) is reaching its limit. Transmissions with capacities in the order of petabit per second have already been demonstrated using multi-core fibers (MCFs) with single mode transmission in each core. The performance of these systems is limited by the intercore crosstalk (ICXT). This dissertation analyzes the impact of the ICXT as a constraining element of the capacity of coherent detection optical communication networks that use the flexible grid over the C-band. The total capacity of the link, which is given by the number of cores allowed of a weakly-coupled (WC) MCF for each modulation format, is imposed by the maximum mean ICXT power acceptable for the connection. Link impairments such as the wavelength dependence of ICXT power over the transmission band and the nonlinear interference (NLI) noise due to MCF non-linear effects are also considered in the analysis. The total data capacities for metro networks, regional networks and long-distance networks are assessed for a W-profile MCF supported communication links. Considering the impairments of the link as the wavelength dependence of ICXT power over the transmission band and the NLI effects, the total capacities of 483.84 Tb/s by 32-QAM, 430 Tb/s by 32-QAM and 206.08 Tb/s by 4-QAM are achieved for the metro (represented with a link distance of 50 km), regional (represented with a link distance of 500 km) and long-distance networks (represented with a link distance of 5000 km), respectively.

Keywords: Intercore crosstalk, Modulation formats, Multi-core fiber, Optical networks, Space division multiplexing.

Contents

List of Figures

List of Tables

List of Acronyms

ASE - Amplified Spontaneous Emission

BER - Bit Error Rate

CD - Cladding Diameter

CT - Cladding Thickness

DSP - Digital Signal Processing

DWDM - Dense Wavelength Division Multiplexing

EDFA - Erbium-Doped Fiber Amplifier

FM-MCF - Few-Mode Multi-Core Fiber

ICXT - Intercore Crosstalk

ITU-T - Telecommunication Standardization Sector of International Telecommunication Union

LO - Local Oscillator

MCF – Multi-core Fiber

MIMO - Multiple-Input Multiple-Output

MMF - Multi-Mode Fiber

NLI - Nonlinear Interference

OSNR - Optical Signal-to-noise Ratio

PDM – Polarization Division Multiplexing

PSD - Power Spectral Density

QAM - Quadrature Amplitude Modulation

ROADM - Reconfigurable Optical Add-Drop Multiplexers

SCI - Self-Channel Interference

SC-MCF – Strongly Coupled Multi-core Fiber

SDM - Space-Division-Multiplexing

SM-SCF - Single-Mode Single Core Fiber

TA-MCF - Trench-Assisted Multi-Core Fiber

WC-MCF - Weakly Coupled Multi-Core Fiber

WDM - Wavelength Division Multiplexing

XCI - Cross-Channel Interference

List of Symbols

α - fiber loss coefficient

β – fiber propagation constant

β_2 – group velocity dispersion

γ - fiber nonlinearity coefficient

σ_1 - wave number in the cladding along the transversal direction

λ - wavelength of light in a vacuum

$\Lambda_{m,n}$ - distance between cores n and m

Δ_1 - relative refractive index difference between the core and the cladding

Δ_2 - relative refractive index difference between the trench and the cladding

Δf_t - bandwidth of channel t

$\Delta ICXT_{dB}$ - relative mean ICXT power

$\Delta OSNR$ – OSNR penalty

Δv_{ch} - channel spacing

a_1 - core radius

a_2 - inner cladding radius

a_3 - distance from the outer edge of the trench to the core center

B_{av} - total available bandwidth per core

B_{ref} - reference bandwidth

B_s - bandwidth of the slot frequency

B_{tot} - total bandwidth per WDM channel

C - bit rate for each single channel

C_{tot} - total capacity per core

d_{amp} - distance between optical amplifiers

$d_{\max}$ - maximum distance between neighbouring cores in a WC-MCF

$d_{\min}$ - minimum distance, between neighbouring cores in a WC-MCF

D_{λ_0} - fiber dispersion parameter at wavelength λ_0

erfc(x) - complementary error function

f_n - amplifier noise figure

f_t - central frequency of channel t

g_k - gain of the optical amplifier k

$G_{NLI}\left(f_t\right)$ - PSD of NLI noise of channel t over multiple spans

$G_{SCI}^{lspan}\left(f_t\right)$ - PSD of SCI of channel t over a span

$G_{XCI}^{lspan}\left(f_t\right)$ - PSD of XCI of channel t over a span

h - Planck constant

$I_0(x)$ - zero order modified Bessel function of the first kind

$J_0(x)$ - zero order Bessel function of the first kind

$J_1(x)$ - first order Bessel function of the first kind

$K_1(x)$ - first order Bessel function of the second kind

K - wave number

k_{mn} - mode coupling coefficient between core m and n

L – MCF length

n_0 - refractive index of the cladding

n_1 - refractive index of the core

n_2 - refractive index of the trench

N_{amp} - number of amplifiers

N_b - number of bits carried in each symbol

N_c - number of inner circles

N_{ch} - number of WDM channels available per core

N_{GB} - number of guard-band slots

N_s - number of slots per channel

$N_{s,tot}$ - total number of slots available for a particular core

N_{spans} - number of spans

$osnr_{modified}$ - modified OSNR

$OSNR_{req}$ - required OSNR under real conditions

$osnr_{req,i}$ - required OSNR under ideal conditions

P_0 - target outage probability

P - average signal power at the end of the fiber link over the two states of polarizations

p_{ch} - optimal launch power

p_{NLI} - NLI power at the end of the fiber link

$P_{b_{M-QAM}}$ - bit error probability of the M-QAM modulation format

R_b - bending radius

r_{ic} - radius of the inner circles

r_{oc} – radius of the container

R_s - symbol rate

snr_b- signal-to-noise ratio per bit

S_{ASE_k} - PSD of the ASE noise of the *k-th* amplifier for the two states of polarization

$S_{ASE_{tot}}$ - total PSD of the ASE noise in the two states of polarizations

S - slope of the relative mean ICXT power

V_1 - normalized frequency

ν_i - channel optical frequency

W_1 - normalized transverse wave number

w_{tr} - trench thickness

X_M - total mean ICXT power considering the relative mean ICXT power in core m induced by all the cores in the fiber

x_{mn} - statistical mean of the ICXT power

$x_{m,n,\Delta ICXT}$ - mean ICXT power considering the relative mean ICXT power (in dB) in core m induced by core n

X_N - total mean power of ICXT in core n

$XT_{\mu,thres}$ - ICXT threshold level

$XT(\Delta OSNR)$ - ICXT level for a maximum allowed OSNR penalty

Chapter 1

Introduction

1.1 Motivation and context

The worldwide-experienced traffic growth is of up to 24% each year [1]. Optical networks have a fundamental role supporting this trend. The transmission capacity limits of conventional single-mode single core fiber (SM-SCF) has increased enormously over time, due to the combination of coherent detection, dense wavelength division multiplexing (DWDM), digital signal processing and enhancement of the spectral efficiency, reaching its limit around 100 Tb/s over a distance of 240 km [2, 3]. However, this limit may no longer support the future worldwide traffic demands. In order to face this issue and achieve ultra-high capacity transmission, space-division-multiplexing (SDM) has been proposed [4, 5]. Over the years, SDM technologies have demonstrated great potential to produce ultra-high capacity long-haul communication transport systems [6]. For example, the trans-oceanic class ultra-long-haul transmission using multi-core fiber (MCF) has achieved the capacity-distance product exceeding 1 Eb/s·km, using a 7-core MCF over a distance of 7326 km [7].

In SDM transmission systems, several independent signals are transmitted simultaneously by providing multiple spatial channels along a single fiber, and can be accomplished, with a multi-mode fiber (MMF), a MCF or a few-mode multi-core fiber (FM-MCF) [2]. The simplest form of realizing SDM is to aggregate SM-SCF in a bundle or SM-SCF ribbon cables. In the MMFs, multiple spatial paths along a single fiber are achieved with the use of multiple different modes inside the fiber [2]. The MCFs have

multiple separate cores in the cladding and each core operates as an independent waveguide. The FM-MCF consists in a combination of both, where only a small number of modes is propagated in each core. The FM-MCF is an attractive way to achieve dense SDM since it can increase the capacity using the multiplicity of the core and mode. A capacity around 3 Pb/s was demonstrated using a 12 cores with 3 modes FM-MCF [8].

SDM using MCF is one of the most investigated solutions to accomplish future worldwide traffic demands [7, 9-12]. MCF have been proposed as a way to reach the demanded capacity for ultra-long-haul transmission [7], radio access networks [10], optical access networks [11] and inter-data center optical communication networks [12]. Space on the undersea cable is limited and for this reason MCFs can be attractive to increase capacity. In this work, homogeneous weakly-coupled (WC) MCFs are considered. WC-MCFs are fibers with a low core density and distance between two neighbouring cores around 40 μm [2]. In homogeneous WC-MCFs, all the cores are nearly identical which simplify the design of the transmitter and receiver [13]. The homogeneous WC-MCFs support high spectral efficiency modulation formats and wideband operation and they do not need of complex high-order multiple-input multiple-output (MIMO) based receivers [14]. In short term, homogeneous WC-MCFs using coherent detection may offer the simplest migration path for adoption of high-capacity SDM technology since they require less drastic changes to transmitter and receiver hardware [14, 15].

The transmission of several parallel signals inside the fiber leads to intercore crosstalk (ICXT) between cores. The ICXT effect is a potential limitation of SDM systems [14, 16-18]. In order to allow high capacity and long distance, ICXT suppression has become a prime concern in WC-MCF coherent systems [9, 16-19]. Since the SM-SCF may no longer support the traffic demands and being the MCFs systems one of the more promising solutions, the performance of these systems is at the limit imposed by ICXT, so it is very important to investigate the limits of the capacity of the WC-MCF coherent systems imposed by the ICXT, in particular, their dependence on the location of the cores, distance between cores as well as the best modulation format in order to have higher data rates networks.

1.2 Goals and research questions

The main goal of this dissertation is to study the capacity limits of ICXT-limited WC-MCFs coherent systems. In conventional SM-SCF, the core is placed at the center of the cladding with 125 μm cladding diameter (CD). In MCFs, the core layout, the core design, the number of cores, the cladding thickness (CT) (which is the distance between outermost core center and the cladding edge [20]) and CD can be optimized from the view point of optical and mechanical properties in order to minimise the ICXT level and maximise the capacity of the link [21]. So, it is imperative to understand the physical parameters as the distance between neighbour cores, number of cores and refractive index of the MCFs that affect the ICXT level and its impact on the transmission capacity, distance and performance.

When the number of cores increases, the capacity of the transmission increases but the ICXT also increases. So, it is necessary to realize in what extent this relationship works to maximise the transmission capacity for different distances for a given CD. The number of cores in the cladding depends on the core arrangement, distance between neighbour cores and CT [2, 21].

In this dissertation, WC-MCFs are considered. To minimize ICXT, it is necessary to analyse and optimize the cores location regard the MCF physical parameters. After that optimization, the ICXT power and the ICXT threshold level are calculated and the number of cores in the fiber, as well as the best modulation format for different link distances, are assessed in order to maximise the total capacity. Beyond this, the impairments of the link as the wavelength dependence of ICXT power over the transmission band and the nonlinear interference (NLI) effect are also considered and the total capacity is found.

To accomplish this, a software will be developed in MATLAB, which will enable the evaluation of the system capacity impaired by ICXT by varying the MCF physical parameters. The objectives of this dissertation are:

- Study and implementation of a software that allows the core location in the cladding for a given CD, which maximises the distance between cores;

- Estimation of the ICXT power and assessment of the total capacity for different link distances;
- Evaluation of the total capacity for different links distances considering the impairments of the link.

With the objectives set out, the following questions arise:

1. How the main physical parameters (core arrangement, CT, distance between neighbour cores) determine the ICXT magnitude?
2. What is the maximum ICXT allowed in communication systems supported by MCF considering the maximum transmission capacity and distance?
3. What is the variation of the ICXT magnitude using W-profile and trench-assisted WC- MCFs and its dependence on the fiber physical parameters?
4. How does the cores arrangement and other physical parameters of the MCF affect the performance (bit error rate (BER)) of the optical communication system?

1.3 Dissertation organization

The dissertation is structured as follows. In chapter 2, the review of the literature of the most important concepts used in this work is presented. The different types of MCF for SDM application and the impairment in the use of MCF, as known as ICXT are presented. Chapter 2 also describes the coherent detection technique and the flexible grid as well as its advantages.

In chapter 3, the methodology followed to estimate the mean ICXT power for W-profile MCFs is presented. Firstly, the strategy and the method used to obtain the optimum core layout of the W-profile MCF are presented. Secondly, the mode coupling coefficient for homogeneous TA-MCF is calculated and the mean ICXT level is estimated. Afterwards, the mode coupling coefficient and the ICXT level are estimated for the W-profile MCFs.

In chapter 4, the impact of the ICXT power in the capacity of the link is assessed. The number of cores and the modulation format that lead to the maximum capacity are assessed. Additionally, the evaluation of the capacity of the link is made considering the

wavelength dependence of ICXT power over the transmission band and the nonlinear fiber effects.

Chapter 5 concludes this dissertation by presenting the main conclusions of this work and suggestions of future work related to the subject of the dissertation.

1.4 Main original contributions

This work presents the following contributions:

- Assessment of the coupling coefficient and analysis of the mean ICXT power for the W-profile MCF.
- Analysis of the sensitivity of the mean ICXT power to the propagation constant variation.
- Analysis of the transmission capacity and link reach for different *M*-QAM modulation formats in ideal conditions, i.e., where ICXT, NLI effects and ICXT wavelength dependence are not being considered.
- Assessment of the total capacity for different network link distances in the presence of ICXT.
- Assessment of the total capacity considering the NLI effects and the ICXT wavelength dependence.

Chapter 2

Literature Review

The fact that the capacity of SM-SCF will be soon exhausted and with the continuous grow of the worldwide traffic, SDM networks are a good candidate to the future worldwide traffic demands. In this chapter, the review of the literature about SDM networks is presented. The different types of MCF are presented in section 2.2. In section 2.3, the main limiting factor that arises with the use of a MCF, the ICXT, is characterized. The coherent detection technique and its advantages are presented in section 2.4. In section 2.5, the flexible grid and the corresponding frequency grid are presented and the advantages of the use of a flexible grid are described.

2.1 SDM networks

The infrastructure that supports the communications all around the globe has been involving continuously during the last decades and optical networks proved to be the ideal candidate to accommodate the growing demand so far [15]. The world needs to set the bar of network capacity even higher with the appearance of "Big Data", real time gaming, high definition audio-video streaming and other demanding bandwidth applications [15]. However, the physical limits of the SM-SCF capacity will soon be exhausted [2, 3, 15, 22]. Nowadays, the researchers consider SDM as a mean to overcome the capacity crunch [4, 5, 15] and, with that in mind, the first concern was exceeding the capacity limit around 100 Tb/s [22, 23]. The first record capacity achieved was 109 Tb/s over a 16.8 km using

a 7-core MCF [24]. The transmitted signal was 86 Gb/s QPSK with 97 WDM channels. The manufacture of the MCF and SDM multiplexed/demultiplexer devices, which are the connection between the SM-SCFs with the MCF, were the technologies that allowed the record at the time [23]. Free space optics was adopted for WC-MCFs since it is high power capable, adjustable, have low insertion losses and low ICXT. In the same year, the capacity of 112 Tb/s was also achieved [25]. After that achievement, the challenge was to increase the number of cores in the fiber and a capacity of 305 Tb/s over 10.1 km with a 19-core MCF was reached [26]. The research to achieve the greatest capacity and distance have not stopped since then and recently, a capacity of 1.51 Eb/s×km and 4.59 Eb/s×km was reached with a 12-core MCF [27, 28].

The basic concept of SDM is based on placing numerous spatial channels in a given fiber structure or fiber arrangement [15]. The simplest form of realizing SDM is to aggregate SM-SCF in a bundle or SM-SCF ribbon cables and it is already commercialized [15]. The SM fiber ribbon consists in the aggregation of many conventional SM-SCF ranging from tens to hundreds creating a fat fiber bundle or ribbon cable. The diameter of these bundles ranges from 10 mm to 27 mm. Fiber ribbons can transmit over hundreds of parallel links due to its large dimension, which makes it less space efficient [15]. For example, ribbon cables with a diameter of 16 mm and 25 mm can carry 144 (12×12 fiber ribbons) and 864 (36×24 fiber ribbons) SM-SCFs, respectively [29]. This method has already been adopted in current optical fiber infra-structure [15].

Since, for long-haul, core and metro networks, amplification is an essential aspect of a network, integrated SDM amplifiers are an absolute key element towards spatially multiplexed future networks [15]. There are two kinds of pumping scheme in the case of multi-core amplifier: core pumping or cladding pumping. The core pumping is the conventional pumping scheme used for a conventional single core erbium-doped fiber amplifier (EDFA) and provide high pumping efficiency [30]. The challenges to be faced include the integration of optical components to reduce the amplifier size, cost and energy consumption [30]. In the cladding pumping scheme all the cores are pumped by first cladding propagation pump light [30]. The challenges are to improve the pumping efficiency and to develop optical components for launching the pump and multiple signal lights and to adjust the gain of the cores to obtain pump power with high-speed control [30]. The SDM amplifiers, in particular, those that use cladding pump are more energy efficient in contrast to deploying parallel conventional EDFAs for amplification [15]. The

capacity of 110.9 Tb/s over a 6 370 km long link was achieved using a full C band seven core EDFA [31].

Fan-in/Fan-out is the process of coupling a MCF into a SM-SCF or vice-versa and it is one of the aspects that impacts the viability and performance of SDM network [15]. Fan-in/Fan-out can be achieved using direct and indirect coupling methods. The direct method consists in connecting directly the MCF with the SM-SCF with a waveguide-optics interface. The indirect method relies on a lens system and requires sophisticated optomechanics [15].

In order to SDM technology be a viable solution it is necessary to go against the different types of network requirements. Core and metro networks need to be scalable in order to accommodate higher traffic load, to be highly reconfigurable, changing the parameters of the routing and to be resilient , i.e. those networks should be capable of react and provide backup solutions to restore the connections after any failure [15]. In order to face the scalability requirement, SDM reconfigurable optical add/drop multiplexers (ROADM) experimental prototypes have been already demonstrated. Since ROADMS are crucial elements of those networks, these solutions have to be solid. SDM networks are resilient and failure recovery through the many spatial channels that compose the network, i.e., if one channel fails their adjacent can replace it instantaneously. Concerning long-haul networks, the challenges are ICXT as well as amplification, so it is a lot of work on going to reduce the ICXT.

2.2 Classification of multi-core fibers

MCFs for SDM application were firstly proposed in 1979; however, due to their high cost, they were kept out of the market for many years [32]. Nowadays, the future data capacity crunch became an issue, and the SDM approach with MCFs has been widely proposed as a cost effective solution [2, 32, 33] to increase the capacity per cross-sectional area of the fiber, and overcome the foreseen data capacity crunch [32].

MCFs can be classified from the fiber design point of view as:

- Homogeneous MCFs - These fibers have identical cores. All the cores have the same structure, i.e., identical refractive indices, core radius and propagation properties between cores [2, 34].
- Quasi-homogeneous MCFs - A MCF that exhibits cores with slight differences between them regarding the effective refractive indices and propagation constants due to fabrication issues [34].
- Heterogeneous MCFs - A MCF designed to have different propagation constants and refractive indices between the cores which leads to the reduction of the ICXT level [2, 34].

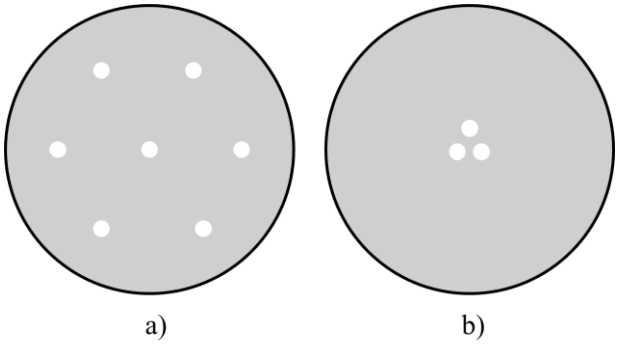

Figure 2.1- a) WC-MCF and b) Strongly-coupled MCF.

MCFs can also be classified int two different categories: WC and strongly-coupled (SC) MCFs, as illustratively shown in Figure 2.1. WC-MCFs are fibers with a distance between two neighbouring cores, defined in the literature as core pitch Λ, around 40 μm and with a low core density [2]. In WC-MCFs, the coupling coefficient between neighbouring cores should be lower than $10^{-2}m^{-1}$. SC-MCFs are fibers with a distance between neighbouring cores shorter than 30 μm which results in a core density increase. In SC-MCFs, the coupling coefficient is around $10^{-1}m^{-1}$ [2]. In this case, MIMO digital signal processing (DSP) with low complexity is required at the receiver side to recover the transmitted signals increasing the complexity of the system [2, 35]. When compared with SC-MCF, WC-MCF is more competitive for cost-sensitive scenarios [35], such as fronthaul for 5G [10], optical access network [11] and inter-data center optical communication networks [12], as MIMO DSP at the receiver side for recovering the signals is not required [2]. Nonetheless, SC-MCF is more advantageous in long-haul transmission scenarios because of their enhanced nonlinear tolerance [35]. Even so, several WC-MCFs have been developed in several works to accomplish high-capacity

long-distance transmission [2, 24, 25, 31, 36]. In this work, the capacity limits are assessed only for WC-MCFs.

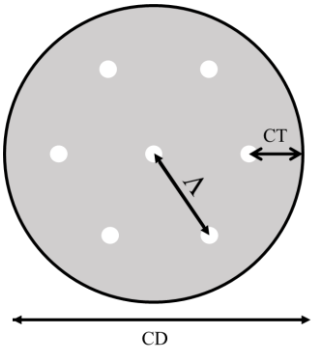

Figure 2.2- Structure of a 7 core WC-MCF with the cores represented in white and cladding represented in grey.

Figure 2.2 shows the structure of a 7-core WC-MCF with a step-index structure, it is composed with cores represented in white and cladding represented in grey in which the cladding has a lower refractive index than the cores. MCFs, typically, have a value of the cladding diameter (CD) ranging from 125 μm to 260 μm which corresponds to the CD of a conventional SM-SCF and to CD that allows the maintenance of the mechanical reliability, respectively [37]. The core pitch, is the distance between two neighbouring cores, Λ, which in this 7-core fiber layout is the same between all cores [16]. The CT is the distance between the outermost core center and the cladding edge as shown in Figure 2.2 [20].

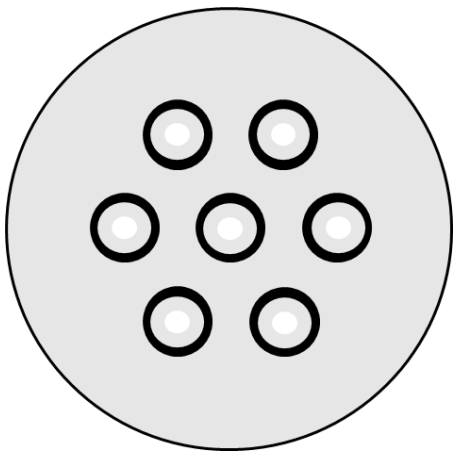

Figure 2.3- Cross sectional view of a homogeneous trench-assisted 7-core MCF, with the cores represented in white, the trenches in black and the inner and outer claddings in grey.

Figure 2.3 shows the structure of a homogeneous 7-core trench-assisted (TA) WC-MCF. The TA-MCF are composed for the cores represented in white, and the inner cladding which is the layer around the core represented in grey, the trenches represented in black around the inner cladding and the outer cladding represented in grey. These fibers have a lower-index trench layer around the inner cladding that surrounds each core [2], as shown in Figure 2.3, which results in a reduction of the coupling coefficient and, consequently, in a reduction of the ICXT level due to the overlap of the electromagnetic fields between cores. TA-MCFs have been widely proposed to reduce the ICXT level compared with a step-index MCF [2, 17].

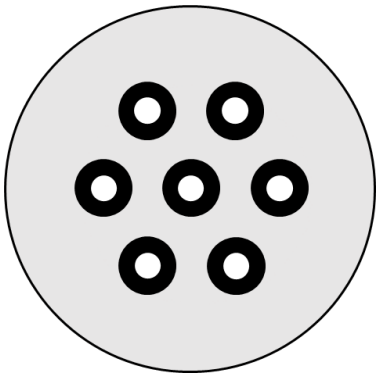

Figure 2.4- Cross sectional view of a W-profile 7-core MCF, where the cores are represented in white and the trenches are represented in black.

Figure 2.4 shows the structure of a W-profile MCF. The W-profile fiber emerged to improve the limitations of a SM-SCF, such as it larger attenuation, smaller core radius and higher dispersion [38]. The W-profile MCF consists in a fiber with an index layer around each core with the refractive index lower than the core and the cladding [38]. The W-profile MCFs can achieve the highest spatial spectral efficiency ever fabricated in SM MCFs for a transmission distance up to 4000 km [39]. The W-profile MCF structure was used to achieved a throughput of 2.15 Pb/s over 31 km with 22 cores reported in [36].

2.3 Intercore crosstalk

The ICXT is a critical transmission issue in MCF supported links [40] because the transmission of a signal inside a core induces interference on the signal in other core. The ICXT has a stochastic behaviour, i.e., the ICXT varies randomly over time and

wavelength [14] and can be understood as a residual amount of the optical signal power transmitted in one of the fiber cores that is coupled to adjacent cores along propagation in the MCF[16].

In WC-MCFs, the ICXT level depends mainly on the distance between neighbouring cores [14], i.e., the ICXT level increases with the decrease of the distance between two neighbouring cores. Moreover, a higher core count is desirable in order to increase the capacity of the link. However, for a given CD, higher core counts lead to lower distances between neighbouring cores, which leads to a higher ICXT level in WC-MCFs [16]. Therefore, there is a trade-off relationship between low ICXT level and high core count [41]. Thus, the core layout and the maximum number of cores have to be carefully designed based on the suitable ICXT level [2]. Also, in WC-MCFs, the core-to-core ICXT is directly dependent on the fiber length and wavelength , i.e., the ICXT level increases for longer distances and for higher values of wavelength [16].

The suppression of ICXT is a critical issue for MCF implementation [41] and has become a major concern in WC-MCF research, in order to achieve the desired high capacity and long distance transmission [17-19, 42]. In order to reduce the ICXT level, TA-MCFs have been proposed [17, 41]. In TA-MCFs, the ICXT level is reduced by the trench layer around each core (with the refractive index lower than the refractive index of the cladding), hence, alleviating the trade-off between low ICXT level and higher core count. Heterogeneous MCF is another effective way to reduce the ICXT level through the differences between the propagation constant, refractive index and radius of different cores. The technique of propagation-direction interleaving was also proposed to suppress ICXT in WC-MCFs [18], which consists on transmitting signals in opposite propagation directions assigned to neighbouring cores and the amount of ICXT suppressed depends significantly on the core arrangement [18].

The performance of SDM transmission systems using WC-MCFs may be limited by the ICXT, which is related to the distance between neighbouring cores, the cores location and transmission distance [43]. Thus, in WC-MCFs, the optimization of the core layout performs a significant role in ICXT suppression and, simultaneously, in maximizing the capacity through the increase of the number of cores.

2.4 Coherent optical communications

Coherent transmission and DSP provided over the past few years a huge advance in higher spectral efficiency and capacity [44, 45]. MCF transmission with coherent detections allows to improve significantly the transmission capacities of the actual long-haul communications and therefore is a very promising transmission technology [46].

Coherent detection is a detection technique where the optical signal recovered contains the amplitude and the phase information, allowing the greatest flexibility in modulation formats used [47]. High order modulation formats are supported in optical coherent detection systems, such as *M*-ary quadrature amplitude modulation (QAM) or *M*-ary phase shift keying signals, since the information can be encoded in both in-phase and quadrature components, which consequently, increases the spectral efficiency without increasing the spectral bandwidth [44, 48]. The spectral efficiency report how efficient the bandwidth is utilized in terms of transmitted information and it is expressed in b/s/Hz [44]. The coherent receiver is composed by a local oscillator (LO) in which the signal is coupled with the incoming signal [45]. There are three types of coherent detection: homodyne detection, intradyne detection and heterodyne detection. The homodyne technique is the most complex, requires the exact synchronization of the incoming signal frequency and the LO. In intradyne detection, the frequency of the incoming signal is very similar with the frequency of the LO. In this case, it is necessary the use of a free-running LO in order to synchronize the signals. In heterodyne detection, the incoming signal and the LO have different frequencies and the optical signal is demodulated to an intermediate frequency. This technique requires a wider bandwidth although the implementation is simpler than the homodyne detection.

Coherent detection combined with polarization-division multiplexing (PDM) technique, which consists in transmitting two modulated signals in the same optical carrier frequency but with orthogonal polarizations, doubles the spectral efficiency of a given modulation format without requiring additional optical signal noise ratio (OSNR) [48, 49]. The signals in the two polarizations can be recovered through a coherent detector receiver by digitizing the received signal and processing it in the digital domain. [48, 49].

Coherent detection increases the receiver sensitivity when compared with direct detection. Since both amplitude and phase of the optical signal are recovered, it is possible

to compensate for linear transmission effects. So, with coherent detection, the receiver can digitally compensate for transmission impairments such as chromatic dispersion and polarization mode dispersion, which are limiting factors for higher bit rate in optical fiber transmission [44, 49].

As optical coherent detection allows higher order modulation formats and it can be combined with PDM, this technique is the chosen one for the implementation of higher data rates networks [45, 48]. Most MCF-based SDM systems have so far considered coherent detection. For example a capacity of 112 Tb/s was achieved by a 9-core MCF over 76.8 km with PDM-QPSK signals [25] and also a capacity of 2 Pb/s with a 22-core homogenous MCF over a 31 km was reached using coherent detection [36].

The optical coherent transmission systems are limited by the generation of nonlinear interference (NLI) as well as the amplified spontaneous emission (ASE) noise accumulation [50]. The NLI occurs due to the Kerr effect in the fiber which induce nonlinear waveform distortion and limit the maximum distance of high-order modulation formats [45, 50]. The ASE noise results from the use of optical amplifiers, since they produce ASE with signal amplification [51].

2.5 Flexible Grid

The capacity requirements of optical networks are characterized for the emerging heterogeneous and bandwidth intensive applications. It is of the most importance to make advantage of the low network resources, as the fiber bandwidth, and accommodate the dynamic traffic demands [52]. In order to do that, the flexible optical grid networking concepts has been proposed [52].

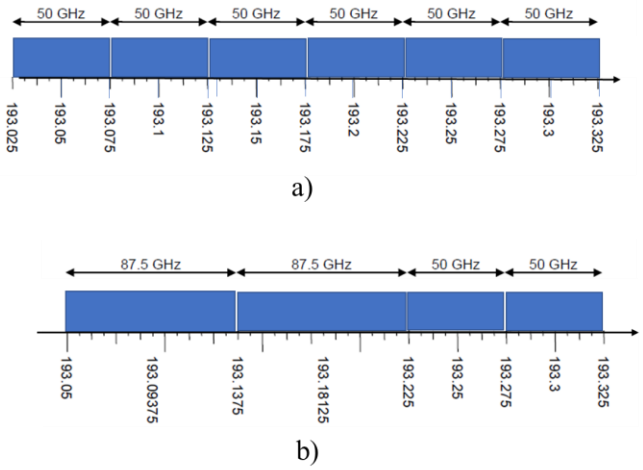

Figure 2.5 – a) the 50 GHz fixed grid spacing and an b) example of flexible grid

Figure 2.5 shows the 50 GHz fixed grid spacing and an example of the use of the flexible grid. The 50 GHz wavelength grid divides the optical spectrum range of 1530–1565 nm (C-band) into fixed 50 GHz spectrum slots [53]. In conventional wavelength division multiplexing (WDM) based networks, the fixed bit rates are of 10, 40 and 100 Gb/s. The channels are modulated with a fixed modulation format [52]. Flexible grid networks are able to adjust its resources, such as the optical bandwidth and the modulation format according to the requirements of each connection, which leads to an efficient utilization of the spectrum resources [52, 54]. The grid spacing can be flexible and not limited to the fixed 50 GHz spacing as shown in Figure 2.5. Nowadays, the flexible grid/SDM network scenario is more and more appealing given its huge bandwidth capacity and its ability to efficiently accommodate low bit rates light paths and high bit rate super-channels together [55]. The flexible optical grid enables the formation of super channels, which consist of several densely packed subcarriers [52].

In this work, the flexible grid is considered. The capacity of the optical fiber is increased with the use of the flexible grid due to the optimization of the usable bandwidth [56]. Following the recommendation given by the Telecommunication Standardization Sector of International Telecommunication Union (ITU-T) [56], the allowed frequency slots for a flexible DWDM grid have a nominal central frequency (in THz) given by

$$\nu_i = 193.1 + n_i \times 0.00625 \qquad \text{[THz]} \qquad (2.1)$$

where n_i is an integer and 0.00625 is the nominal central frequency granularity in THz. The slot width, B_s, (in GHz) is given by [56]:

$$B_s = 12.5 \times m_i \text{ [GHz]} \tag{2.2}$$

where m_i is a positive integer and 12.5 is the slot width granularity in GHz.

The capacity-distance product exceeding 1 Eb/s×km was achieved using a 7 core homogeneous WC-MCF with a transmission capacity of 140.7 Tb/s over a 7326 km using a flexible grid over the C-band [57].

Chapter 3

Estimation of the mean crosstalk power in WC-MCFs

In this chapter, the core arrangement and the estimation of the mean ICXT power for TA-MCF and W-profile MCF are presented. In section 3.1, the strategy for the distribution of the cores in the cladding is described. The method to obtain the optimum core layout for a different number of cores is presented in section 3.2. In section 3.3, the minimum and maximum distances between neighbouring cores are calculated. In section 3.4, the structure of a TA-MCF is presented. In section 3.5, the mode coupling coefficient as well as the propagation constant are calculated for homogeneous TA-MCFs. In section 3.6, the mean ICXT power level for TA-MCFs is estimated. Sections 3.7, 3.8 and 3.9 repeat the procedures shown in sections 3.4, 3.5 and 3.6 for the structure of a W-profile MCF, respectively.

3.1 Packing circles inside a container

The ICXT level in a WC-MCF is highly dependent on the distance of the neighbouring cores. Therefore, the core arrangement has a preponderant role on the capacity limits of the link [43]. In order to maximise the distance between neighbour cores and obtain the minimum ICXT level, the distribution of the cores in the cladding should be carefully designed. As the core layout design is a similar problem than the well-known problem of

packing circles in a circle [58], in the present work, the distribution of the cores in the cladding follows the one proposed in [59].

The problem of circular packing that consists on the arrangement of a finite number of circles inside a container without overlapping is addressed in [59]. This approach consists in maximising the density of the inner circles by maximising their radius given that the container (the outer circle) area is fixed. The density of the inner circles is the ratio between the total area occupied by the inner circles and the container area. The solutions for the packing problem presented in [59] are defined in a bi-dimensional space (x,y). The container has a fixed-sized radius (r_{oc}) equal to one and its center is located at (0,0). The number of inner circles (N_c) is comprised between 1 and 2604. In this work, values for N_c between 2 and 50, which are typically the ones found in MCFs [43] are considered.

For each N_c, the solution to the packing problem presented in [59] returns

- the inner circle coordinates (x_j,y_j), where j is the index of the circles ranging between 1 and N_c;
- the radius of the inner circles (r_{ic});
- the ratio defined as the inverse of the radius ($1/r_{ic}$);
- the density of the inner circles;
- the number of loose circles, which is the number of circles that still have degrees of freedom for movement inside the container, i.e., the number of circles which do not have contact with any other circle;
- the boundary, which is the number of inner circles in contact with the container;
- the number of contacts which corresponds to the boundary plus the number of contacts between the inner circles themselves;

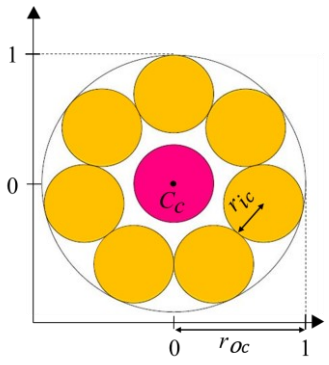

Figure 3.1- Optimum packing of 8 circles.

As an example, Figure 3.1 shows the optimum packing of 8 circles, as presented in [59]. Moreover, when N_c is equal to 8, there is one loose circle, the pink circle, which has some degree of freedom for movement in the container, as shown in Figure 3.1. The value of r_{ic} is equal to 0.3025933 and the value of r_{oc} is equal to 1. For this case the boundary is 7, the number of contacts is 14, the density of the inner circles is 0.7325021 and the ratio is 3.3047649 as indicated in [59].

3.2 Transformation of the coordinates of the inner circles centers into the coordinates of the corresponding cores of a real WC-MCF

In order to obtain the structure of a WC-MCF with an optimal layout of cores following the locations presented in [59], it is necessary to transform the coordinates of the centers of the inner circles in the container in metric coordinates corresponding to the centers of the cores inside a WC-MCF with a given cladding diameter.

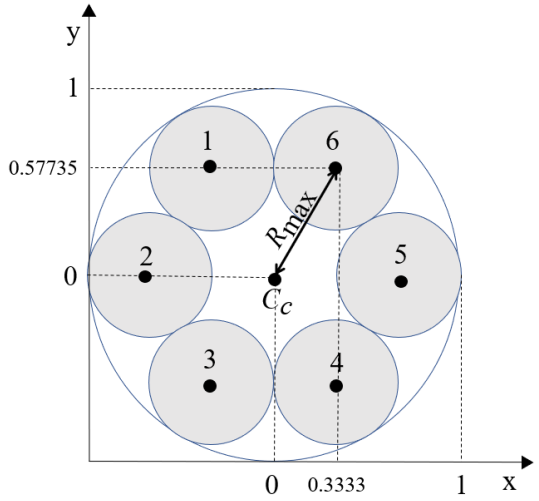

Figure 3.2-Container packing with 6 inner circles and its centers representation as well as the center of the container C_c.

The inner circles center coordinates (Figure 3.2) are converted to the coordinates of the center of the cores of a real WC-MCF as follows:

i) Using the inner circles center coordinates (x_j, y_j) taken from [59], the distance (R_j) between each inner circle and the center of the container is computed by

$$R_j = \sqrt{x_j^2 + y_j^2} \tag{3.1}$$

ii) The next step consists in finding the maximum distance R_j, i.e., the $R_{\max}$ as shown in Figure 3.2. In this work, the parameter $R_{\max}$ ranges from 0.5 to 0.8142, corresponding to $N_c = 2$ and $N_c = 50$, respectively.

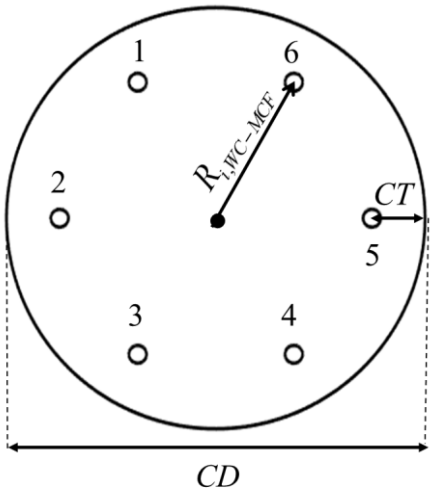

Figure 3.3- Structure of a 6-core WC-MCF.

Figure 3.3 shows the core layout of a 6-core WC-MCF. The parameter $R_{i,WC-MCF}$, which corresponds to the distance between the center of the fiber and the outermost core center, as shown in Figure 3.3 is given by

$$R_{i,WC-MCF} = \frac{CD}{2} - CT \tag{3.2}$$

where *CD* is the cladding diameter and the *CT* is the thickness of the cladding.

In the structure of a WC-MCF, the distance $R_{i,WC-MCF}$ (Figure 3.3) corresponds to $R_{\max}$ (Figure 3.2). We define the proportionality constant K_{N_c} between $R_{\max}$ and $R_{i,WC-MCF}$ as

$$K_{N_c} = \frac{R_{i,WC-MCF}}{R_{\max}} \tag{3.3}$$

Using K_{N_c}, we can obtain the coordinates of the cores (X_j, Y_j) from the coordinates of the inner circles (x_j, y_j) by:

$$(X_j, Y_j) = K_{N_c} \times (x_j, y_j), \; j = 1, ..., N_c \qquad (3.4)$$

The physical parameters of the homogeneous WC-MCFs considered in this work are summarized in Table 3.1.

Table 3.1- Physical parameters of WC-MCFs.

Parameters	Acronym	Value	Units
Cladding diameter	CD	260	µm
Cladding thickness	CT	33	µm
Core radius	a_1	5.5	µm

The values of the physical parameters presented in Table 3.1 were taken from [43] in order to compare the results obtained.

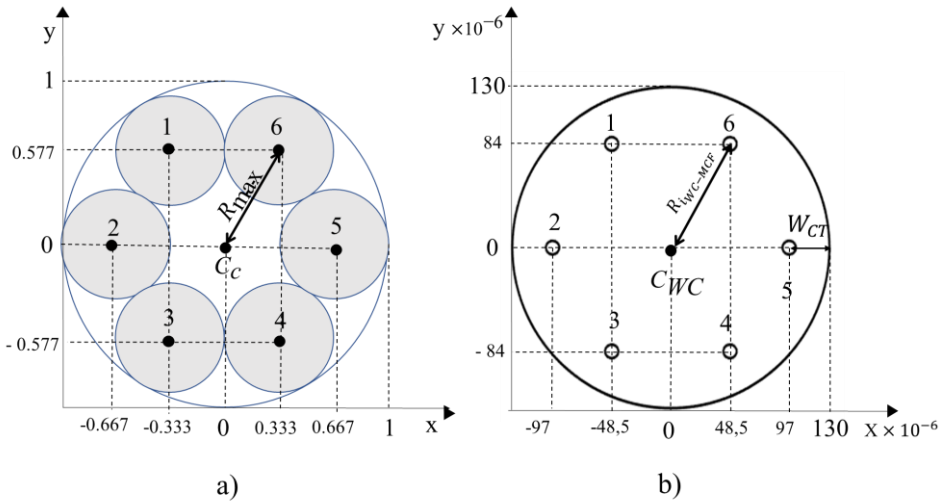

Figure 3.4- a) Packing with 6 inner circles and its coordinates representation b) representation of a WC-MCF with 6 cores and their respective coordinates.

Figure 3.4 shows the transformation of the coordinates of the 6 inner circles given by [59] (Figure 3.4- a)) into the coordinates of the centers of the cores of a real WC-MCF

structure (Figure 3.4- b)). Figure 3.4- b) is an example of an optimal core layout for a WC-MCF with 6 cores achieved with the method described in this chapter.

3.3 Determination of minimum and maximum distances between neighbour cores

The distance between core *n* and *m*, $\Lambda_{m,n}$ is given by

$$\Lambda_{m,n} = \sqrt{(x_n - x_m)^2 + (y_n - y_m)^2} \tag{3.5}$$

where (x_n, y_n) and (x_m, y_m) are the center coordinates of core *n* and *m*, respectively. This distance is particularly important when core *n* and *m* are neighbours. Neighbour cores are the closest cores, i.e, given core *n*, its neighbour cores are the cores that are at the shortest distance when compared to the others, denoted by $\min \Lambda_{m,n}$. The minimum distance, often defined as core pitch in the literature, between neighbour cores in a WC-MCF is given by

$$d_{\min} = \min_m \{\min \Lambda_{m,n}\} \tag{3.6}$$

where *n* and *m* represent all the cores in a WC-MCF with $n \neq m$.

The maximum distance between neighbour cores in a WC-MCF is given by

$$d_{\max} = \max_m \{\min \Lambda_{m,n}\} \tag{3.7}$$

where *n* and *m* represent all the cores in a WC-MCF with $n \neq m$.

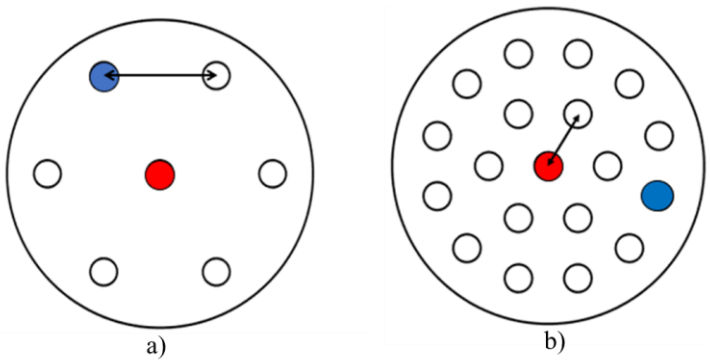

Figure 3.5- Representation of some cores that suffer the maximum (cores in red) and the minimum (cores in blue) mean power of ICXT from a cross section view of a WC-MCF with a) 7 and b) 19 cores whereas d_{min}=d_{max}..

Figure 3.5 shows the optimum core arrangement for a WC-MCF with 7 (Figure 3.5 a)) and 19 (Figure 3.5 b)) cores as, indicated in [59]. The physical parameters used are summarized in Table 3.1 and the distance between the cores was calculated using Equation (3.5). In both fiber layouts, the distances between neighbour cores are equal. Therefore, $d_{\min}$ is equal to $d_{\max}$. In a 7-core WC-MCF (Figure 3.5 a)) $d_{\min}$ and $d_{\max}$ are equal to 92 µm and in a 19-core WC-MCF (Figure 3.5 b)))) $d_{\min}$ and $d_{\max}$ are equal to 47.62 µm. Although the distances between neighbouring cores are equal, in these fibers it is expected that the cores coloured in red suffer more ICXT power since they have more adjacent neighbours in comparison with the other cores in that fiber. For example, in a 7-core WC-MCF (Figure 3.5 b)), the red core has six neighbours in comparison with the outer cores that have only three. In Figure 3.5, the blue cores are an example of the cores that suffer less ICXT power in that fiber. Since $d_{\min}$ and $d_{\max}$ are equal the cores that suffer less ICXT power are the ones that have less adjacent neighbours.

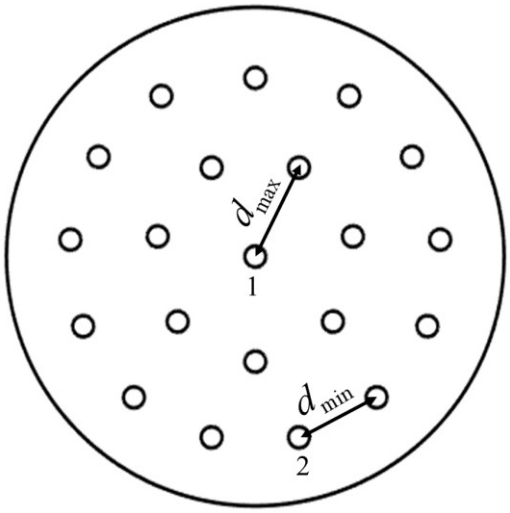

Figure 3.6- Structure of a 21-core WC-MCF with maximum and minimum distances between neighbour cores represented.

Figure 3.6 shows the optimum core arrangement for a WC-MCF with 21 cores with the maximum and minimum distances between neighbour cores represented. Core number 1 is the one that is at longest distance from their neighbours with $d_{\max} = 51.7$ µm. Core number 2 is one of the cores that have the minimum distance from their neighbours, with $d_{\min}$ around 45.6 µm.

The smaller is the distance between neighbour cores, the higher is the coupling coefficient and, consequently, the higher is the mean ICXT power. Considering the distance between neighbour cores and the layout of the cores on a homogeneous WC-MCF, it is possible to know which cores suffer the maximum and minimum ICXT power. It is expected that the core (or cores), that suffers the maximum mean ICXT power is the one with the minimum distance (d_{min}) from its neighbours and the maximum number of neighbours at this distance. The core (or cores) that suffers the minimum mean ICXT power corresponds to the core with the maximum distance (d_{max}) from its neighbours and the minimum number of interfering cores at this distance.

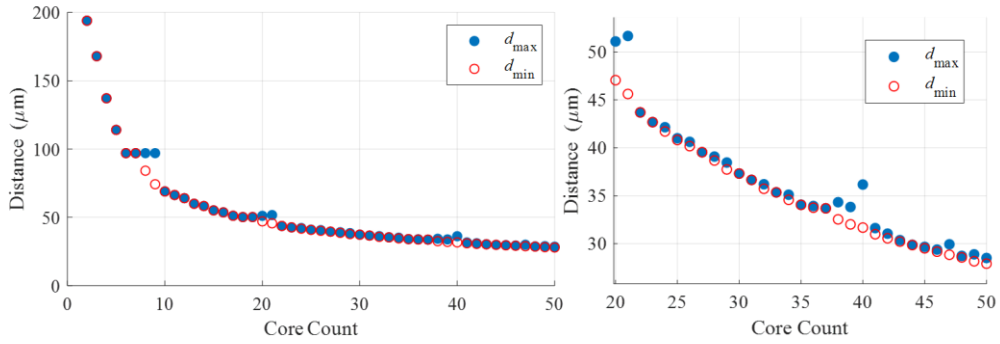

Figure 3.7- a) Minimum and maximum distances between neighbour cores as a function of the core count using the physical parameters of WC-MCFs presented in Table 3.1 b) Zoom in of the previous plot for the core count higher than 20.

Figure 3.7 shows the relation between the minimum and maximum distances between neighbour cores as a function of the core count, for a WC-MCF with the physical parameters presented in Table 3.1. As expected, the distance between neighbour cores is lower for higher core counts. For each core of a particular core count (or core layout), the distance between that core and all the other cores inside the MCF was calculated using Equation (3.5). Afterwards, the minimum and maximum distances between neighbour cores were calculated according to Equations (3.6) and (3.7). The more significant difference between the maximum and minimum distances between neighbour cores occurs when the number of cores is equal to 8, 9, 20, 21 and 40 as shown in Figure 3.7 a) and b). Therefore, these are the cases that is expected to have a higher difference between the minimum and maximum mean powers of ICXT. Figure 3.7 shows that different core counts can lead to the same minimum and maximum distances between neighbour cores.

For example, the structures with 6 and 7 cores, have the same maximum and minimum distance between neighbour cores, equal to 97 µm. This happens because, in these cases, the cladding follows a perfect hexagonality design for the optimal core layout and the difference between those two core distributions is a core in the middle of the cladding, keeping the distance between neighbour cores unchanged. Even though the distance is the same, it is expected that the mean ICXT power to be different because in the 7-core WC-MCF, since the number of interfering cores is higher than in the 6-core WC-MCF.

3.4 Structure of a homogeneous TA-MCF

In a TA-MCF, each core is surrounded by a trench layer with refractive index lower than the cladding. The overlap of electric field between neighbour cores is lower because the electric field distribution in each core is suppressed by the index trench [17] which results on a reduction of the mean power of ICXT compared with a step-index structure. TA-MCFs have been highly proposed for reducing the coupling coefficient and consequently reducing the mean power of ICXT [2, 17].

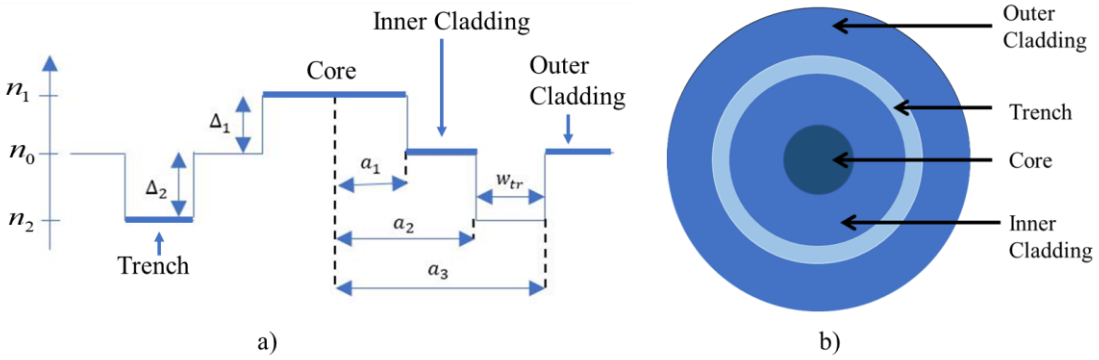

Figure 3.8- a) Refractive index profile around a core of a TA-MCF and b) its cross sectional view.

Figure 3.8 shows the structure around a core of a TA-MCF. The refractive indices of the cladding, the core and the trench are n_0, n_1 and n_2, respectively. The inner cladding is the part of the cladding that surrounds each core as shown in Figure 3.8-b) and have the same refractive index than the outer cladding which is the cladding around the trench. The relative refractive index difference between the core and the cladding is Δ_1. The

relative refractive index difference between the trench and the cladding is Δ_2. The refractive index is given by $n_x = (1+\Delta_x)n_0$ with $x=1$ or 2. The core radius, the distance from the outer edge of the inner cladding to the core center (inner cladding radius), the distance from the outer edge of the trench to the core center and the trench thickness are a_1, a_2, a_3 and w_{tr}, respectively. The trenches of neighbour cores should be carefully designed, so they do not overlap [60]. For the design of TA-MCF, it is important to consider the ratio between a_1 and a_2, since there is a trade-off in the placement of the trench ($a_3 = a_2 + w_{tr}$) [60]. On one hand, the effective area of each core will be reduced if the trench is placed too close to the core [60]. On the other hand, the trench should be placed as close as possible to the core to reduce the distance between neighbour cores to increase the MCFs core density [60].

A TA-MCF is homogeneous when all the cores have the same structure, i.e., when all the cores have the same values of a_1, a_2, a_3 and w_{tr}, as well as the corresponding refractive indices. However, the process of the fabrication of an optical fiber leads to minor fluctuations of its structure originating a quasi-homogeneous TA-MCFs. These imperfections produce a variation of the propagation constant that affects the mean power of ICXT.

3.5 Mode coupling coefficient and propagation constant calculation for homogeneous TA-MCFs

The mode coupling coefficient in TA-MCFs is written as [60]:

$$k_{mn} = \frac{k(n_1^2 - n_0^2)W_1 U_1 L_q}{n_1 a_1^2 V_1^2 J_1^2(U_1)} \sqrt{\frac{\pi a_1}{2W_1 \Lambda_{m,n}}} \exp\left[-\frac{W_1}{a_1}\Lambda_{m,n}\right] \cdot \int_0^{a_1} J_0\left(\frac{U_1}{a_1} r\right) \times I_0\left[\left(\frac{W_1}{a_1} + \frac{P_1 - P_2 + Y_1 - Y_2}{\Lambda_{m,n} - r}\right) r\right] \exp\left(-\frac{P_1 - P_2 + Y_1 - Y_2}{\Lambda_{m,n} - r}\Lambda_{m,n}\right) r dr \quad (3.8)$$

where $k = 2\pi/\lambda$ is the wave number and λ is the wavelength of light in vacuum. In Equation (3.8), $W_1 = \sqrt{a_1^2(\beta^2 - k^2 n_0^2)}$; $U_1 = \sqrt{a_1^2(k^2 n_1^2 - \beta^2)}$; β is the propagation constant; $V_1 \simeq k a_1 n_1 (2\Delta_1)^{1/2}$ and determines the number of modes propagating in the cores; $J_1(x)$ is

the first order Bessel function of the first kind, $J_0(x)$ is the zero order Bessel function of the first kind and $I_0(x)$ is the zero order modified Bessel function of the first kind.

The parameters L_q, P_1, P_2, Y_1, Y_2 can be expressed as [60]

$$L_q = \frac{J_1(U_1)K_1(W_1a_2/a_1)K_1(W_2a_3/a_1)}{K_1(W_1)K_1(W_2a_2/a_1)K_1(W_1a_3/a_1)} \tag{3.9}$$

$$P_1 = W_1\frac{\Lambda_{m,n}-a_3}{a_1} \tag{3.10}$$

$$P_2 = W_2\frac{\Lambda_{m,n}-a_3}{a_1} \tag{3.11}$$

$$Y_1 = W_2\frac{\Lambda_{m,n}-a_2}{a_1} \tag{3.12}$$

$$Y_2 = W_1\frac{\Lambda_{m,n}-a_2}{a_1} \tag{3.13}$$

$$P_1 - P_2 + Y_1 - Y_2 = \left(W_2 - W_1\right)\frac{a_3-a_2}{a_1} = \left(W_2 - W_1\right)\frac{w_{tr}}{a_1} \tag{3.14}$$

where $K_1(x)$ is the first order Bessel function of the second kind and $W_2 = \left(V_2^2 + W_1^2\right)^{1/2}$, in which $V_2 = ka_1\left(n_0^2 - n_2^2\right)^{1/2}$.

The mode coupling coefficient in TA-MCF can be further approximated as (these calculations are presented in Appendix A):

$$k_{mn} \simeq \frac{\sqrt{\Gamma}\sqrt{\Delta_1}}{a_1}\frac{U_1^2}{V_1^3K_1^2(W_1)}\sqrt{\frac{\pi a_1}{W_1\Lambda_{m,n}}}\exp\left[-\frac{W_1\Lambda_{m,n}+2\left(W_2-W_1\right)w_{tr}}{a_1}\right] \tag{3.15}$$

where $\Gamma = \dfrac{W_1}{W_1 + (W_2 - W_1)w_{tr}/\Lambda_{m,n}}$.

The statistical mean of the ICXT power (x_{mn}) is given by [60]

$$x_{mn} \approx \frac{2k_{mn}^2R_b}{\beta\Lambda_{m,n}}L \tag{3.16}$$

where R_b is the bending radius and L is the fiber length.

The value of parameter β is calculated accordingly with [42]. Taking into account that the wave number in the cladding along the transversal direction is given by

$$\sigma_1 = \sqrt{\beta^2 - n_0^2 k^2} \tag{3.17}$$

The normalized frequency (V_1) is given by [42]

$$V_1 = k a_1 \sqrt{\left(n_1^2 - n_0^2\right)} \tag{3.18}$$

The normalized transverse wave number in the cladding (W_1) can be expressed as follows [42]:

$$W_1 = a_1 \sigma_1 \simeq 1.1428 V_1 - 0.996 \tag{3.19}$$

Combining Equation (3.19) and Equation (3.17), the parameter β is given by

$$\beta = \sqrt{\sigma_1^2 + n_0^2 k^2} = \sqrt{\left(\frac{1.1428 V_1 - 0.996}{a_1}\right)^2 + n_0^2 k^2} \tag{3.20}$$

The parameters of the TA-MCFs used in this work are summarized in Table 3.2, with β calculated using Equation (3.20).

Table 3.2- Parameters of the TA-MCFs for mean ICXT power calculation.

Parameters	Values	Units
a_1	4.5	μm
a_2/a_1	2	-
a_3/a_1	3	-
w_{tr}	a_1	-
n_0	1.45	-
Δ_1	0.35	%
Δ_2	-0.35, -0.7	%
R_b	140	mm
B	5.8928×10^6	1/m

The parameters presented in Table 3.2 for the TA-MCFs are taken from [60] in order to confirm the results obtained with the software developed in Matlab. Since, we consider homogeneous TA-MCFs all the cores are identical, i.e., the values of the parameters a_1, a_2, a_3, w_{tr}, n_0, Δ_1 and Δ_2 are equal for all cores.

3.6 Estimation of the mean crosstalk power level for TA-MCFs

In order to ensure the proper calculation of Equations (3.8) and (3.15) the coupling coefficient was computed under the same conditions considered in [60], particularly, those considered to obtain Figure 3 of [60]. The TA-MCF parameters considered to compute the coupling coefficient are presented in Table 3.2.

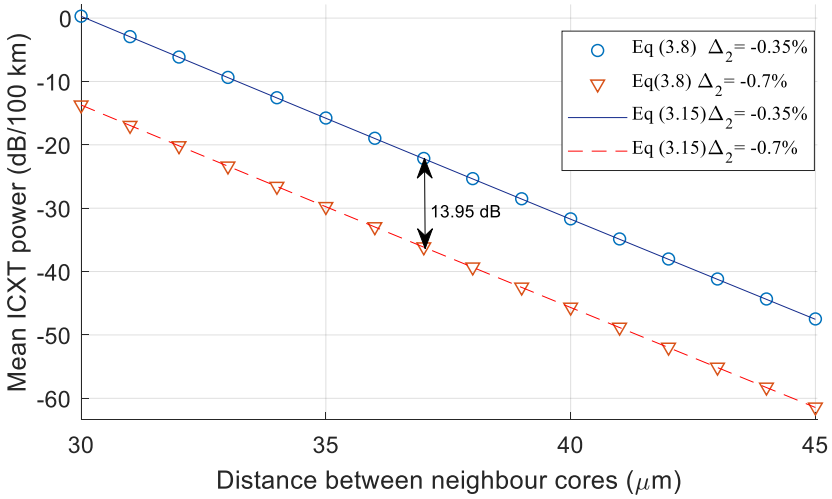

Figure 3.9- Mean ICXT power in dB as a function of the distance between neighbour cores in a TA-MCF for the parameters presented in Table 3.2 for a total fiber length of 100 km.

Figure 3.9 shows the mean ICXT power as a function of the distance between neighbour cores for the TA-MCF with parameters presented in Table 3.2. Equations (3.8) and (3.15) are correctly implemented given that the results shown in Figure 3.9 are in agreement with the Figure 3 presented in [60]. The slight difference between the results presented in Figure 3.9 and Figure 3 of [60] is due to the different values of the propagation constants. In this work, the propagation constant is calculated accordingly with [42], while in [60], the value of the propagation constant is not explicitly presented. However, this difference is not relevant, since it is below 1 dB. Figure 3.9 shows a decrease of the mean ICXT power of 3 dB/μm with the increased distance between neighbour cores.

3.7 Structure of a homogeneous W-profile MCF

A W-profile structure is used in order to compare the results obtained with the results presented in [43].

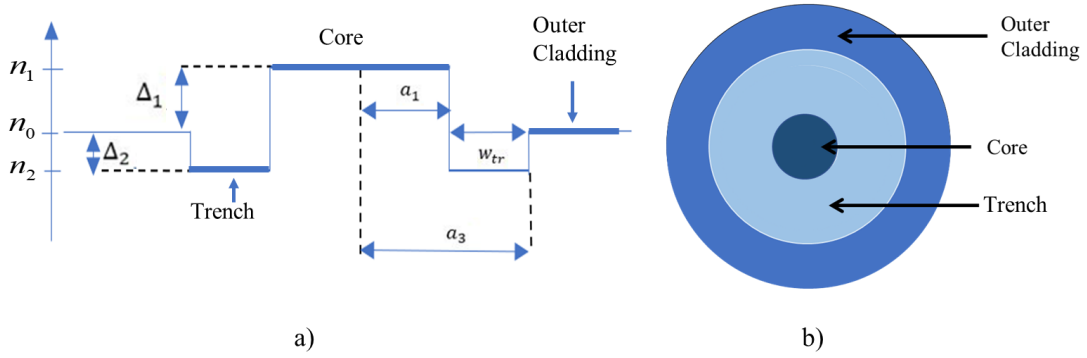

Figure 3.10 – a) Refractive index profiles around a core of a W-profile MCF and b) its cross sectional view.

A W-profile fiber is composed of the core, the trench and the outer cladding, as shown in Figure 3.10. A W-profile MCF is homogeneous when all the cores have the same structure, which means that all the cores have the same values of a_1, a_3 and w_{tr}, as well as the same refractive indices.

3.8 Calculation of mode coupling coefficient for homogeneous W-profile MCFs

For a W-profile MCF, $a_1 = a_2$ and $w_{tr} = a_3 - a_1$. Thus, the mode coupling coefficient of a W-profile MCF can be written, approximately, as:

$$k_{mn} \simeq \frac{\sqrt{\Gamma}\sqrt{\Delta_1}}{a_1} \frac{U_1^2}{V_1^3 K_1^2(W_1)} \sqrt{\frac{\pi a_1}{W_1 \Lambda_{m,n}}} \exp\left[-\frac{W_1\Lambda_{m,n} + 2(W_2 - W_1)(a_3 - a_1)}{a_1}\right] \quad (3.21)$$

The parameters of the W-profile MCFs used in this work are summarized in Table 3.3.

Table 3.3- Parameters of a W-profile MCF for the mean ICXT power calculation.

Parameters	Values	Units
a_1	5.5	µm
a_2	a_1	µm
a_3	12	µm
w_{tr}	6.5	-
n_0	1.44	-
Δ_1	0.4	%
Δ_2	-0.13	%
R_b	140	mm
L	1	km

The parameters presented in Table 3.3 for the homogeneous W-profile MCFs are taken from [43] in order to compare the results obtained with the ones presented in Figure 1 b) of [43].

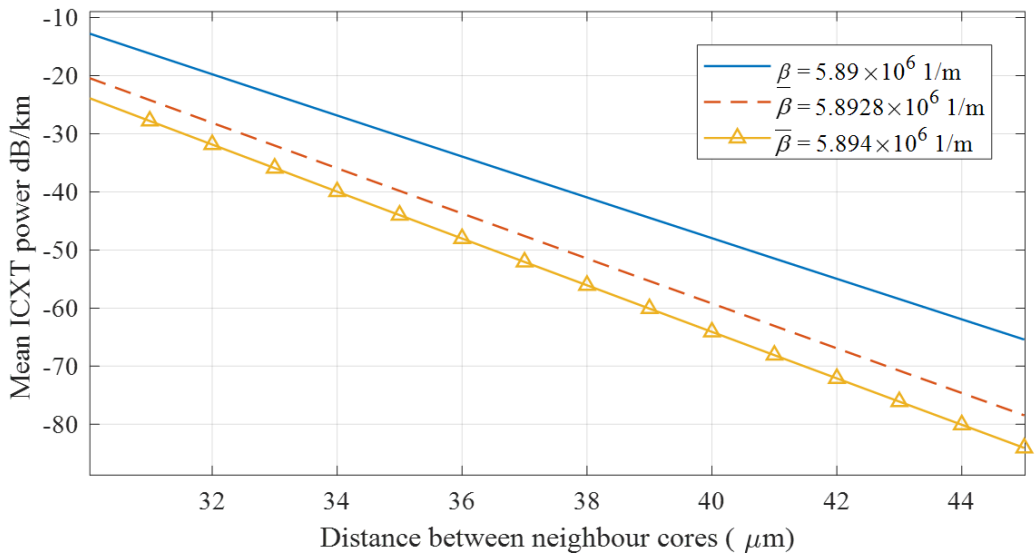

Figure 3.11- Mean ICXT power per unit of length in dB/km as a function of the distance between neighbour cores of a W-profile MCF with the parameters presented in Table 3.3.

Figure 3.11 shows the mean ICXT power as a function of the distance between neighbour cores in a W-profile MCF for different values of β. The parameter $\beta = 5.8928 \times 10^6$ 1/m was calculated through Equation (3.20) and is represented by the red line. In order to assess the influence of parameter β in the relationship between the mean ICXT power and the distance between neighbour cores, two different values of β, $\underline{\beta} = 5.890 \times 10^6$ 1/m and $\overline{\beta} = 5.894 \times 10^6$ 1/m, which correspond to a decrease of 0.0475%

and to an increase of 0.0203 % of the β, respectively have been considered. As shown in Figure 3.11, for equal distances between neighbour cores, lower values of β lead to higher mean ICXT power, whereas higher values of β lead to lower mean ICXT power. For instance, when the distance between neighbour cores is equal to 30 µm, the difference of the mean ICXT power between $\underline{\beta} = 5.89\times10^{6}$ and $\beta = 5.8928\times10^{6}$ is around 7 dB and when the distance between neighbour cores is equal to 45 µm this difference is around 13 dB. So, the slight variation of β induces a significant variation of the mean ICXT power.

As shown in Figure 3.11, it is possible to observe the sharp decrease of the mean ICXT power when the distance between neighbour cores increases. For $\beta = 5.8928\times10^{6}$, Figure 3.11 shows a decrease of the mean ICXT power of 4 dB/µm with the distance between neighbour cores increase.

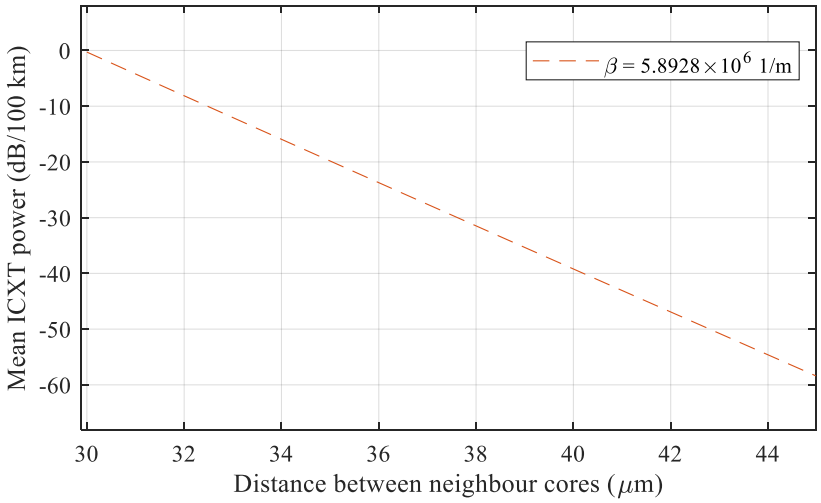

Figure 3.12- Mean ICXT power in dB/100km as a function of the distance between neighbour cores of a W-profile MCF with the parameters presented in Table 3.3.

Figure 3.12 shows the mean ICXT power as a function of the distance between neighbour cores in a W-profile MCF for a link distance of 100 km with the structural parameters presented in Table 3.3 in order to compare with the TA-MCF represented in Figure 3.9 with the structural parameters presented in Table 3.2. For the distances between neighbour cores considered in both Figures, a TA-MCF with $\Delta_2 = -0.7\%$ shows better results, i.e., presents lower values of the mean ICXT power for the same distances between neighbour cores than a W-profile MCF. The TA-MCF with a $\Delta_2 = -0.35\%$

have the same value of the mean ICXT power of 0 dB for a distance between neighbour cores of 30 μm. However, the W-profile MCF shows better results when the distance between neighbour cores increases. For example, when the distance between neighbour cores is equal to 45 μm, the mean ICXT power for a W-profile MCF is -58 dB, whereas for a TA-MCF it is around -48 dB.

3.9 Estimation of the crosstalk level for a W-profile MCF

The mean ICXT power given by Equation (3.16) considers only the interference between two cores. The total mean power of ICXT in core *n* takes into account the contributions from all the cores of the MCF and is given by

$$X_N = \sum_{m \neq n} x_{m,n} \tag{3.22}$$

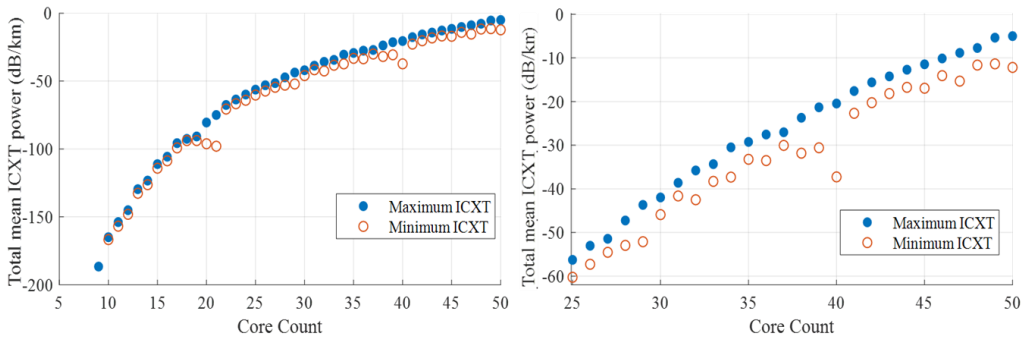

Figure 3.13- a) Maximum and minimum total mean ICXT powers in dB/km as a function of the core count for W-profile MCF using the structural parameters presented in Table 3.3 b) Zoom in for the previously plot for core count higher than 25.

Figure 3.13 shows the maximum and minimum total mean ICXT powers in a W-profile MCF as a function of the number of cores ranging from 2 to 50, using the parameters presented in Table 3.3. For each core, the distance between core *n* and any other core was calculated using Equation (3.5), followed by the calculation of the corresponding coupling coefficient using Equation (3.21). Afterwards, the mean ICXT power induced on that core by another core is calculated using Equation (3.16). Finally, through Equation (3.22) the total mean ICXT power induced on that core is calculated. Figure 3.13 is, then,

a representation of the maximum and minimum total mean ICXT power as a function the core count. The total mean ICXT power increases with the core count as expected. As shown in Figure 3.11, the mean ICXT power for a distance between neighbour cores around 39.5 μm is, approximately, -57 dB. This distance occurs when N_c is around 27, as shown in Figure 3.7. The ICXT power is around -57.28 dB for a distance between 2 neighbour cores of 39.5 μm calculated using Equation (3.16) which are in accordance with Figure 3.11. Furthermore, the cores that suffer the maximum mean ICXT power have 4 neighbour cores distanced by 39.5 μm. Thus, the ICXT power for this case is around -51.22 dB calculated using Equation (3.22) which are in accordance with Figure 3.13 since the maximum mean ICXT power when N_c is equal to 27 is around -51.4 dB.

In comparison with the Figure[1] 1. b) in [43], there are slight differences between Figure 3.13, namely, when $N_c = 10$, the maximum total mean ICXT power obtained is around -165 dB whereas in Figure 1. b) in [43], it is around -140 dB. When $N_c = 23$, the maximum total mean ICXT power obtained is around -63.5 dB, whereas in Figure 1. b) of [43], it is around -50 dB. Finally, when $N_c = 50$, the maximum total mean ICXT power obtained is around -5 dB, whereas in Figure 1. b) of [43], it is around 1 dB. Since Equation (3.15) is in agreement with [60], and the physical parameters are equal to the ones used in [43], the differences between the figures may likely result from the different β used, because this is the only parameter that is not presented in [43]. Taking this into account, the parameter β was changed in order to obtain a plot with more similarity to the one presented in [43]. The total maximum mean ICXT power is -174 dB for $N_c = 10$ and -8 dB when $N_c = 50$, as shown in Figure 3.13 a) and b), respectively.

[1] The first author of [43] gave the information that the mean ICXT power per km shown in Figure 1. b) of [43] was in dB/km instead of dB/100km.

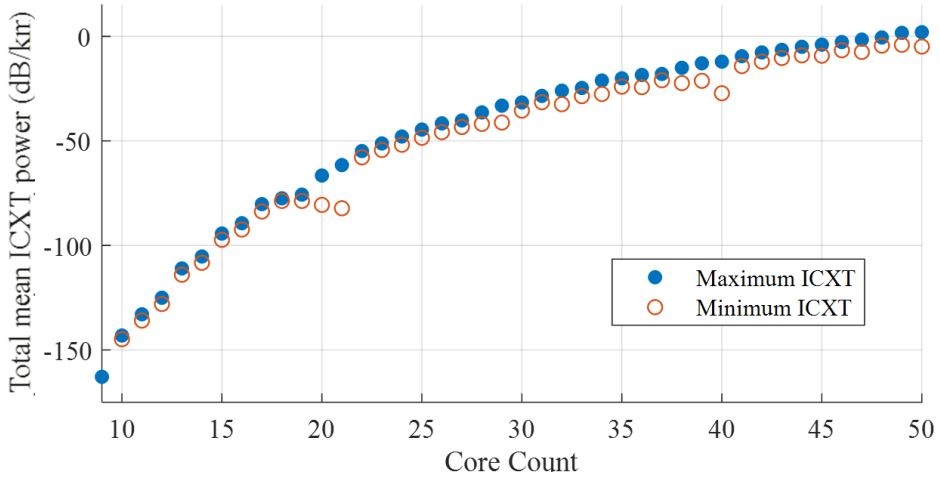

Figure 3.14- Maximum and minimum mean ICXT power in dB/km as a function of the core count with β=5.89×10^6 m^{-1} .

In order to obtain a mean ICXT power closer to the one presented in [43], the parameter β is decreased to 5.89×10^6 m^{-1}. With this value of β, the results presented in Figure 3.14 are obtained. These results are much more similar to the ones presented in Figure 1. b) of [43]. A reduction of 0.0475 % on β results in a difference of 22 dB and 7 dB, when N_c is equal to 10 and 50, respectively. Further simulations have shown that when the parameter β is increased to 5.894×10^6 1/m (an increase of 0.0203 %), for each N_c, the total mean ICXT power decreases in comparison with Figure 3.13 moving away from the values presented in [43]. This reveals that the mean ICXT power is highly sensitive to a variation of the propagation constant.

3.10 Conclusions

In this chapter the method used to pack the cores in the fiber that maximizes the distance between two neighbour cores were presented in order to achieve an optimal core layout. Moreover, the distance between two neighbour cores was evaluated, i.e., this distance decreases with the increase of the core count in the fiber.

Furthermore, the calculation of the coupling coefficient was validated for the TA-MCF. The methodology used to assess the coupling coefficient for the TA-MCF was

adapted for the structure of a W-profile MCF. The maximum and minimum ICXT power for a W-profile MCF were assessed and validated by the works presented in the literature review. The factors that influence the ICXT power in a core are the distance between the neighbour cores and the number of interfering cores. As expected, the main conclusion about the ICXT power behaviour is that for higher core counts the mean ICXT power is higher due to the lower distance between neighbour cores and the higher number of interfering cores.

Additionally, a study was made on the effect that the variation of the propagation constant has on the ICXT power. Our results indicate that the total mean ICXT power is highly sensitive to a variation of the propagation constant.

Chapter 4

Assessment of the networks total capacity

In this chapter, the best modulation format and suitable number of cores that lead to the maximum capacity for metro, regional and long-distance networks are assessed for a W-profile MCF. It is important to evaluate how the impairments affect the capacity of each link. In section 4.1, the achievable transmission capacity is calculated for different modulation formats as a function of the number of cores of the MCF considering only the bandwidth limitation of the C-band. Section 4.2 presents the method used in this work to calculate the required OSNR under ideal and real transmission conditions. In section 4.3, for each distance of the transmission link, the most suitable modulation is determined. In section 4.4, the ICXT threshold level for each modulation format is estimated. In section 4.5, the achievable total capacities for links with distances of 50 km, 500 km and 5000 km are estimated in presence of ICXT. In section 4.6, the relative mean ICXT power for homogeneous W-profile MCFs is calculated considering the wavelength dependence. In section 4.7, the total capacities for link distance of 50 km, 500 km and 5000 km, respectively, considering the relative mean ICXT power dependence on the wavelength are found. In section 4.8, the optimal launch power and the modified OSNR are computed for each modulation format and for different link distances in presence of nonlinear interference noise.

4.1 Transmission capacity calculation for different *M*-QAM modulation formats

M-ary QAM is a multilevel modulation format which exploits the capability of a coherent receiver of detecting the phase and amplitude of the received electric field. In this work, coherent detection with PDM is assumed and the modulation formats considered are 4, 8, 16, 32 and 64. The goal of this section is to find the optimum *M*-QAM that maximises the capacity of a specific link. The bit rate for each single channel, *C*, is considered to be 112 Gb/s. In a QAM modulation format, the number of bits N_b carried in each symbol is given by

$$N_b = \log_2(M) \tag{4.1}$$

where *M* is the number of symbols.

The symbol rate, R_s, is given by [9]

$$R_s = \frac{C}{2\log_2(M)} \tag{4.2}$$

where the factor 2 stands for the two signal polarizations [9].

The total bandwidth per WDM channel, B_{tot} , is assumed equal to the symbol rate since it is considered a Nyquist-shaped PDM carrier [9] and the number of slots per channel (N_s) is given by [9]

$$N_s = \left\lceil \frac{B_{tot}}{B_s} \right\rceil + N_{GB} \tag{4.3}$$

where B_s is the bandwidth of the slot frequency and is assumed equal to 12.5 GHz [9]. The parameter N_{GB} defines the number of slots for the guard-band per connection and it has a bandwidth of 12.5 GHz [9].

The total number of slots $N_{s,tot}$ available for a particular core is given by

$$N_{s,tot} = \frac{B_{av}}{B_s} \tag{4.4}$$

where the parameter B_{av} is the total available bandwidth per core, which is set to 4 THz (C-band) [9].

The number of channels N_{ch} available per core is given by

$$N_{ch}=\frac{N_{s,tot}}{N_s} \tag{4.5}$$

and the total capacity C_{tot} per core is given by

$$C_{tot}=N_{ch}\times C \tag{4.6}$$

In this work, the flexible grid is considered. Following the recommendation given by ITU-T presented in Equation (2.1) and considering that, in this work, the bandwidth of the slots used are 12.5 GHz, the possible nominal central frequencies considered in this work are given by:

$$\nu_i = 193.1 + n_i \times 0.0125 \text{ [THz]} \tag{4.7}$$

where n_i is an integer ranging from -110 to 209, given that the total bandwidth available per core is 4THz and the bandwidth of the slots are 12.5 GHz which results in 320 slots available per core calculated accordingly to Equation (4.4). The lower bandwidth limit was set to 1531.8 nm and corresponds to n_i=209 and the upper bandwidth limit was set to 1564.8 nm and corresponds to n_i=-110.

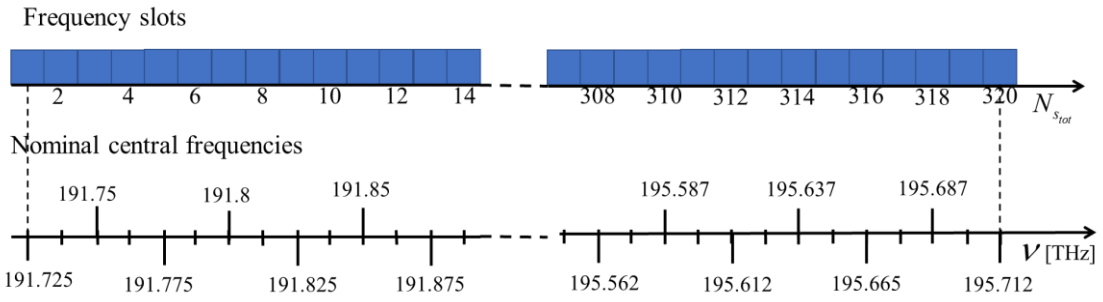

Figure 4.1- Frequency slots and corresponding nominal central frequencies per core.

The upper plot of Figure 4.1 represents the possible frequency slots in a core with a width of 12.5 GHz, whereas the lower plot shows the corresponding nominal central frequencies within the C-band (1531.8 – 1564.8 nm) given by Equation (4.7) anchored to $\nu_0 = 193.1$ THz.

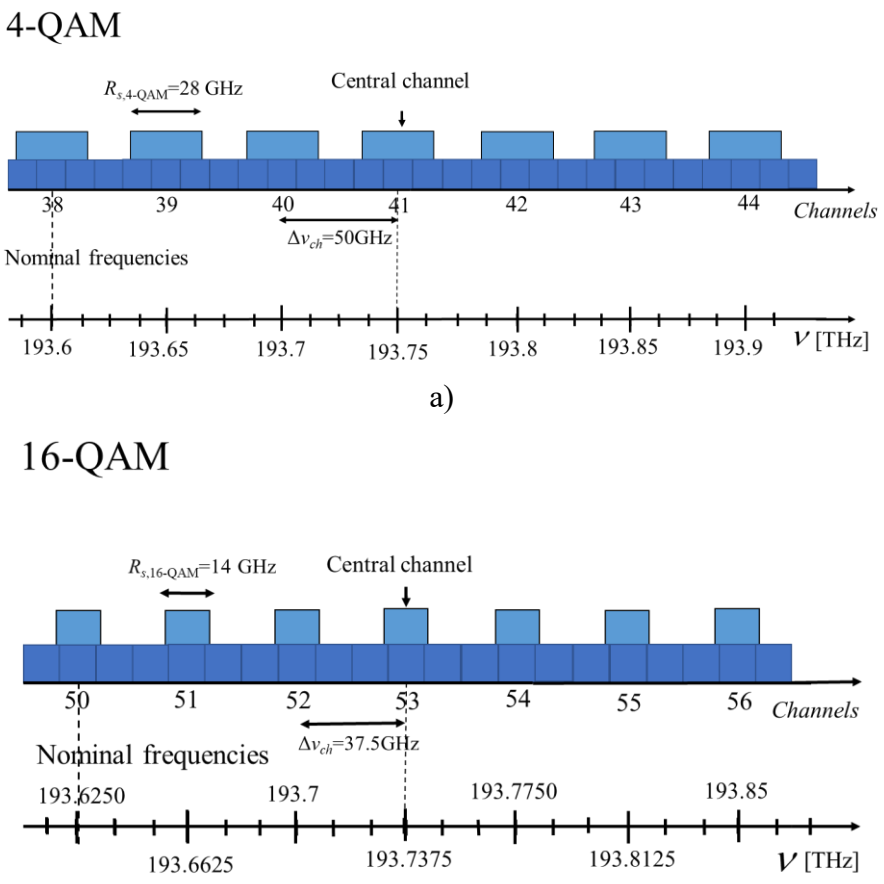

Figure 4.2- Representation of the bandwidth occupied by each channel and their central frequencies for a) 4-QAM and for b) 16-QAM.

Figure 4.2 shows an example of the bandwidth and frequency slots occupied by each WDM signal, nominal frequencies and slot widths for a) 4-QAM channels and b) 16-QAM channels as its central frequencies. The nominal central frequencies for each channel follow the ITU-T recommendation for the flexible grid. The central channel, for each modulation format, was set to $N_{ch}/2+1$. The symbol rate was calculated using Equation (4.2). The number of slots that each WDM channel occupies was calculated using Equation (4.3). The channel spacing (Δv_{ch}) corresponds to the bandwidth of the number of slots that each WDM channel occupies. The nominal central frequencies for each modulation format considered in this work are presented in Appendix B. Table 4.1 summarizes, for each modulation format, the symbol rate, number of WDM channels and the number of slots per channel in the C-band.

Table 4.1- Symbol rate, number of WDM channels and number of slots per channel for each modulation format.

Modulation format	R_s [GHz]	N_{ch}	N_s
4-QAM	28	80	4
8-QAM	18.67	106	3
16-QAM	14	106	3
32-QAM	11.2	160	2
64-QAM	9.33	160	2

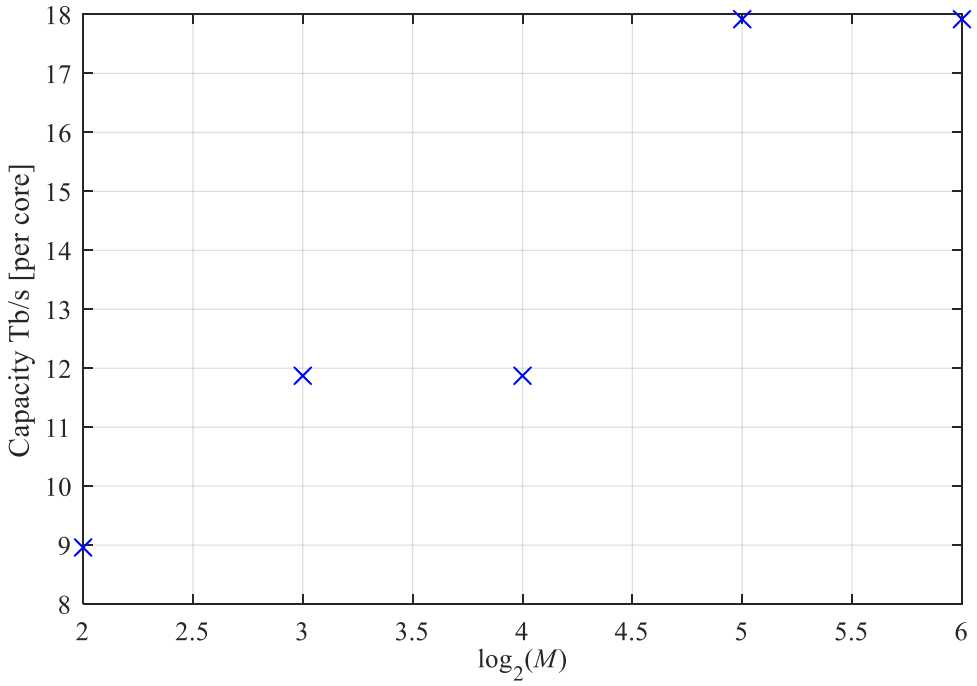

Figure 4.3 – Maximum achievable transmission capacity per core for different M-QAM formats.

In Figure 4.3, the total transmission capacity per core is plotted for different *M*-QAM formats. For each modulation format, the total transmission capacity is calculated using Equations (4.2) -(4.6). The modulation formats 32-QAM ($\log_2(M=5)$) and 64-QAM ($\log_2(M=6)$) lead to the same total capacity, 18 Tb/s, because these modulations achieve the same number of channels in Equation (4.5), 160 WDM channels, since they have the same number of slots per channel, for the system parameters considered. The same explanation applies to the modulation formats 8-QAM and 16-QAM with 106 channels. As shown in Figure 4.3, when *M* increases, the total capacity per core also increases due to the fact that higher order modulation formats allow using more WDM channels. Figure 4.3 only considers the available bandwidth limitation and does not take into account the

effects that limit the capacity of the link such as the ASE noise, the acceptable level of ICXT power, the wavelength dependence of ICXT power over the transmission band or the NLI.

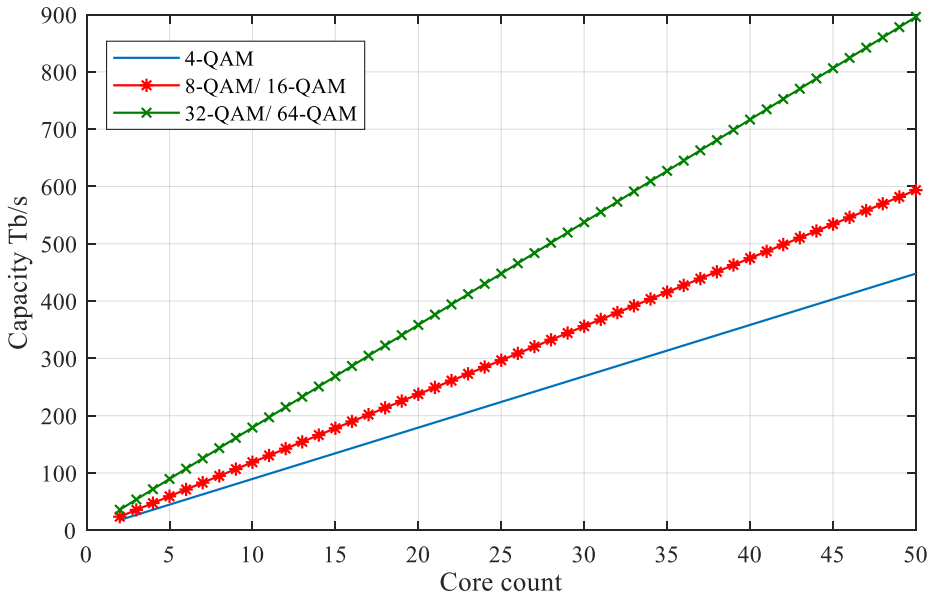

Figure 4.4- Transmission capacity as a function of the number of cores for the different M-QAM formats.

Figure 4.4 plots the total capacity of a MCF as a function of the number of cores for the different modulation formats. Figure 4.4 represents the transmission capacity in ideal conditions, i.e., absence of the ICXT power, the ASE noise, and the NLI. When the number of cores increases, the capacity scales linearly with the number of cores. As shown in Figure 4.4 and according with Figure 4.3, for a core count of 25 and 50 the modulation formats 32-QAM and 64-QAM reach the same total capacity of 448 Tb/s and 900 Tb/s, respectively, where the latter represents the maximum capacity that can be attained with the parameters used in this work. In order to maximise the capacity of the link, the optimal modulation format for this system seems to be the 32-QAM, because it achieves the highest capacity and, when compared with the 64-QAM, allows a greater OSNR margin [61].

4.2 Required OSNR calculation

The required OSNR under ideal conditions, i.e., fluctuations in the network environmental conditions such as temperature, stress and the ICXT effect are not being considered, in linear units, is given by [9]

$$osnr_{req,i} = \frac{C \cdot snr_b}{2 \cdot B_{ref}} \tag{4.8}$$

where snr_b is the required signal-to-noise ratio per bit (in linear units) and B_{ref} is the reference bandwidth typically equal to 12.5 GHz [9, 51] . The analytical bit error probabilities of the *M*-QAM modulation formats considered in this work are given by [47, 61]

$$P_{b_{4-QAM}} = \frac{1}{2}\operatorname{erfc}(\sqrt{snr_b}) \tag{4.9}$$

$$P_{b_{8-QAM}} = \frac{11}{16}\operatorname{erfc}\left(\sqrt{\frac{3snr_b}{3+\sqrt{3}}}\right) \tag{4.10}$$

$$P_{b_{16-QAM}} = \frac{3}{8}\operatorname{erfc}\left(\sqrt{\frac{2snr_b}{5}}\right) \tag{4.11}$$

$$P_{b_{32-QAM}} = \frac{91}{240}\operatorname{erfc}\left(\sqrt{\frac{snr_b}{4}}\right) \tag{4.12}$$

$$P_{b_{64-QAM}} = \frac{7}{24}\operatorname{erfc}\left(\sqrt{\frac{snr_b}{7}}\right) \tag{4.13}$$

with erfc(*x*) defining the complementary error function [47].

The required electrical signal-to-noise ratio per bit snr_b is calculated for the target line BER of 3.8×10^{-3}, which corresponds to the line bit error probability when using hard-decision forward error correction [9, 62]. The values of snr_b are calculated through Equations (4.9)-(4.13) for this target BER. The required OSNRs under ideal conditions are calculated through Equation (4.8).

In order to compute the required OSNR under real conditions, several sources of performance degradation should be taken into account [9]. An OSNR margin of 3 dB is added to account the fluctuations in network environmental conditions such as temperature, stress and other effects [9]. An OSNR penalty of 1 dB is added to the required OSNR under ideal conditions to ensure a margin for the ICXT effect. The required OSNR under real conditions, in dB, is, thus, given by

$$OSNR_{req} = OSNR_{req,i} + 4 \tag{4.14}$$

The values of snr_b, the required OSNR under ideal and real conditions, in dB, for the different modulation formats considering a target BER of 3.8×10^{-3} are presented in Table 4.2. These values are in complete agreement with the ones presented in [9].

Table 4.2- Required snr_b, the required OSNR under ideal and real conditions, in dB, for the different modulation formats considering a target BER of 3.8×10^{-3}.

Modulation Format	SNR_b [dB]	$OSNR_{req,i}$ [dB]	$OSNR_{req}$ [dB]
4-QAM	5.52	12.03	16.03
8-QAM	7.83	14.34	18.34
16-QAM	9.17	15.68	19.68
32-QAM	11.23	17.74	21.74
64-QAM	13.34	19.85	23.85

The *osnr*, in linear units at the optical receiver input, is given by [9, 51]

$$osnr = \frac{P}{S_{ASE_{tot}} \cdot B_{ref}} \tag{4.15}$$

where P is the average signal power at the end of the fiber link summed over the two states of polarizations [51], $S_{ASE_{tot}}$ is the total ASE noise power spectral density (PSD) in the two states of polarizations at the optical receiver input given by [9]

$$S_{ASE_{tot}} = \sum_{k=1}^{N_{amp}} S_{ASE_k} \tag{4.16}$$

where N_{amp} is the number of amplifiers in the link. In this work, it is assumed that each fiber section has an optical amplifier every 50 km. According to [43], the link distances considered, which are representative of typical network links, are 50 km for metro or

access networks, 500 km for regional networks and 5000 km for long-distance networks. The PSD of the ASE noise of the *k-th* amplifier output S_{ASE_k} over the two states of polarization is defined by [9]:

$$S_{ASE_k} = f_n \cdot (g_k - 1) \cdot h \cdot \nu_i \tag{4.17}$$

Where f_n is the amplifier noise figure, g_k is the gain of the optical amplifier, h is the Planck constant equal to $6.62607004 \times 10^{-34}$ J.s and ν_i is the channel optical frequency. It is assumed that each amplifier compensates exactly the losses of the previous fiber link.

The OSNR given by Equation (4.15), at the end of each connection, i.e., at the optical receiver input, should exceed or be equal to the minimum acceptable OSNR, given by Equation (4.14), i.e., to comply with the target BER of 3.8×10^{-3}.

$$osnr \geq osnr_{req} \tag{4.18}$$

The physical parameters used in this work to assess the link performance and feasibility are presented in Table 4.3.

Table 4.3-Values of physical parameters.

Parameter	Value	Units
B_{av}	4	THz
B_s	12.5	GHz
B_{ref}	12.5	GHz
d_{amp}	50	km
N_{GB}	1	
P	0.3	mW
F_n	5	dB
A	0.2	dB/km

In Table 4.3, the parameter d_{amp} is the distance between optical amplifiers and α is the fiber loss coefficient. The parameter α is usually equal to 0.2 dB/km at the wavelength of 1550 nm. The parameter *P* is the average signal power at the optical fiber input and it is assumed low, since a first analysis, the fiber non-linear effects are not taken into account [9]. The values of the physical parameters presented in Table 4.3 are taken from [9].

4.3 Link reach for each modulation format

In order to find the best *M*-QAM modulation format for each distance of the link (or type of network), it is necessary to calculate the required OSNR under real conditions using Equation (4.14) and the OSNR that reaches the optical receiver input, using Equation (4.15), and, then, analyse the modulation formats that accomplish the operating condition given by Equation (4.18), for the parameters presented in Table 4.3.

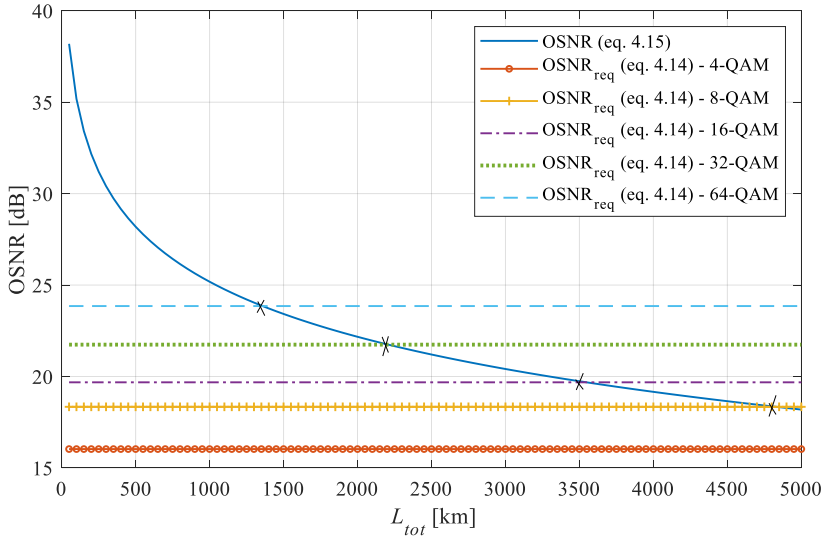

Figure 4.5- OSNR that reaches the optical receiver input as a function of total distance of the link and required minimum OSNRs for the different *M*-QAM modulation formats.

In Figure 4.5, the OSNR that reaches the optical receiver input is depicted as a function of total distance of the link and the required OSNR for each modulation format are also plotted for the different *M*-QAM formats. As shown in Figure 4.5, for 64-QAM, the operating condition is fulfilled up to a total distance of the link of 1358 km, whereas for 32-QAM, 16-QAM and 8-QAM, it is accomplished up to 2208, 3550 and 4830 km, respectively. The modulation format 4-QAM has always the required OSNR lower than the OSNR that reaches the optical receiver, hence, accomplishing the condition presented in Equation (4.18) for the total distance of the link of 5000 km. Taking into account that the total distances of links representing the network types considered in this work are 50 km, 500 km and 5000 km, through the analyses of Figure 4.5, it can be concluded that for a total distance of the link between 50 and 500 km, corresponding to access, metro or

regional networks, all the modulation formats can be used. The best modulation format for these distances is the 32-QAM, since it reaches the same capacity as 64-QAM, but with a higher OSNR margin.

4.4 Determination of ICXT threshold level

For the long term impact of ICXT, it is imposed that the maximum mean ICXT power acceptable for a connection is such that it does not exceed the ICXT threshold level corresponding to the outage probability of 10^{-5} [9]. The ICXT level, in decibel, for a maximum allowed OSNR penalty, $\Delta OSNR$, is defined as

$$XT(\Delta OSNR) = 10\log_{10}\left(1 - \frac{1}{10^{\frac{\Delta OSNR}{10}}}\right) + 10\log_{10}\left(\frac{R_s}{B_{ref}}\right) - OSNR_{req,i} \qquad (4.19)$$

where $OSNR_{req,i}$ is given by Equation (4.14). The ICXT level for a maximum allowed OSNR penalty given by Equation (4.19) is a theoretical result derived in [62].

The ICXT threshold level, in decibel, for a $\Delta OSNR = 1\,\text{dB}$, can be approximated by [9]

$$XT_{\mu,thres} = XT(1dB) - 10\log_{10}\left[0.4431 - \frac{\ln(P_0)}{4}\right] \qquad (4.20)$$

where P_0 is the target outage probability.

The ICXT threshold levels presented in Table 4.4, are obtained for a target outage probability of 10^{-5} and maximum allowed OSNR penalty of 1 dB, for the different modulation formats and for the bit rate per WDM channel equal to 112 Gb/s.

Table 4.4- ICXT threshold levels, in dB, for the outage probability of 1×10^{-5} for different modulation format for a bit rate equal to 112 Gb/s.

Modulation format	$XT_{\mu,thres}$ [dB]
4-QAM	-20.7
8-QAM	-24.77
16-QAM	-27.36
32-QAM	-30.39
64-QAM	-33.29

4.5 Determination of the total capacity for different link distances

The modulation format and the number of cores which lead to the maximum capacity for different link distances are assessed in this section. Considering the outage probability of 10^{-5}, the total capacity of the link is imposed by the maximum mean ICXT power acceptable for a connection that does not exceed the ICXT threshold level. The maximum mean ICXT power is obtained from the results presented in section 3.9, for a W-profile MCF.

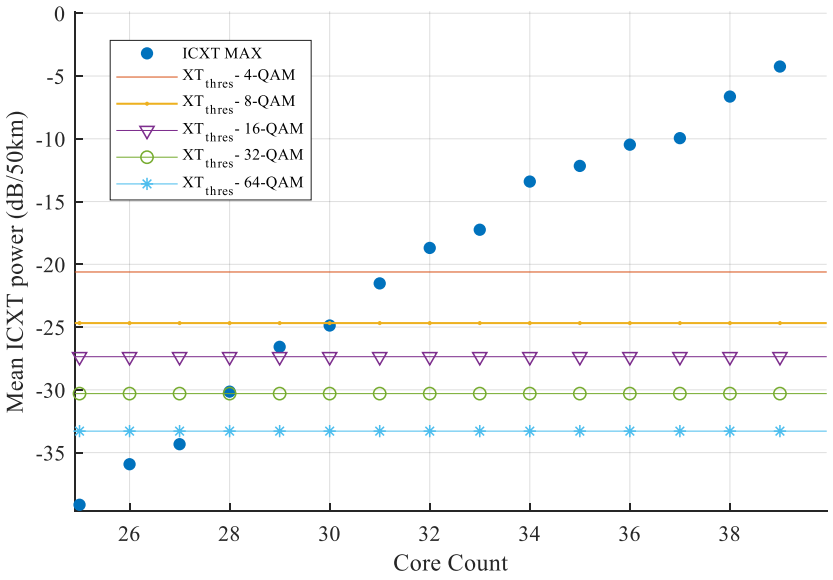

Figure 4.6- Maximum mean ICXT power in dB/50 km as a function of the core count and the crosstalk threshold level for the different modulation formats.

The maximum mean ICXT power in dB/50 km as a function of core count is represented in Figure 4.6, as well as the ICXT threshold levels for 4-QAM, 8-QAM, 16-QAM, 32-QAM and 64-QAM modulation formats, shown in Table 4.4. As mentioned in section 4.3, all the modulations formats accomplished the operating condition given by Equation (4.18) for a total distance of the link equal to 50 km. Table 4.5 summarizes the possible number of cores and the corresponding total capacity, for each modulation format, considering that the ICXT threshold has to be higher than the maximum mean ICXT power. The maximum allowed number of cores is extracted from Figure 4.6.

Table 4.5- Allowed number of cores for a WC-MCF for each modulation format for a fiber length of 50 km considering the crosstalk threshold given in Table 4.4 and the corresponding capacity.

Modulation format	Number of cores	Capacity	Units
4-QAM	31	277.76	Tb/s
8-QAM	30	356.16	Tb/s
16-QAM	28	332.4	Tb/s
32-QAM	27	483.84	Tb/s
64-QAM	27	483.84	Tb/s

As shown in Table 4.5, the highest capacity of 483.84 Tb/s is achieved by the 32-QAM and the 64-QAM with 27 cores in the W-profile MCF. For a length of 50 km, our results indicate that the best modulation format is the 32-QAM since it presents a greater OSNR margin than the 64-QAM modulation format and reaches the highest total capacity. The results presented in [43] reveal that for metro access networks the optimal core count ranges from 23 to 30 cores, being in agreement with our results. However, since the ICXT power considered in this work is lower than the one presented in [43], the optimal core count is 31 for the 4-QAM modulation format.

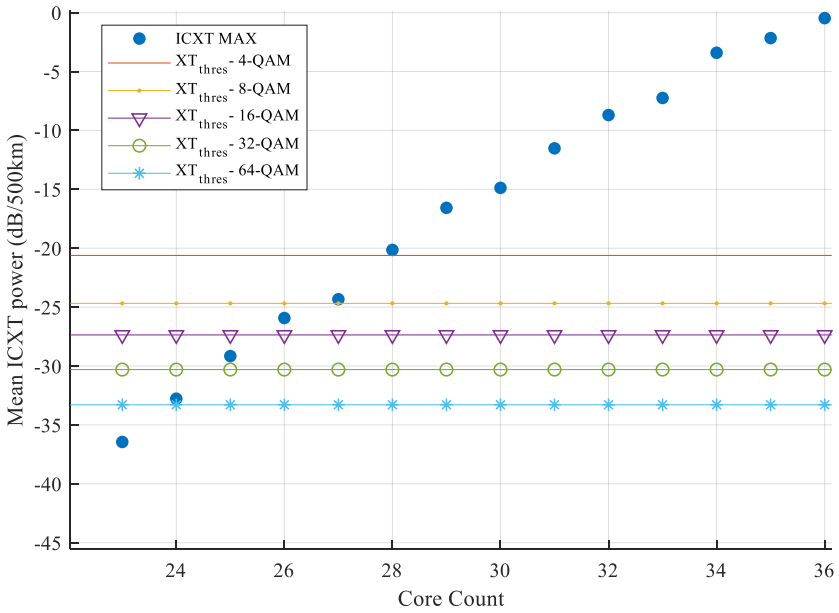

Figure 4.7- Maximum mean ICXT power in dB/500 km as a function of the core count and the ICXT threshold level for the different modulation formats.

The maximum mean ICXT power in dB/500 km as a function of core count is represented in Figure 4.7 as well as the ICXT threshold levels for 4-QAM, 8-QAM, 16-QAM, 32-QAM and 64-QAM modulation formats shown in Table 4.4. All the modulations formats accomplished the operating condition given by Equation (4.18) for a total distance of the link equal to 500 km (as shown in section 4.3). The number of cores allowed for each modulation format, considering that the ICXT threshold level has to be higher than the maximum mean ICXT power, are summarized in Table 4.6 and these values are taken from Figure 4.7. Table 4.6 also shows the total capacity attained for the different modulation formats that corresponds to the maximum number of cores for a fiber length equal to 500 km.

Table 4.6- Allowed number of cores for a WC-MCF for each modulation format for a fiber length of 500 km taking into count the ICXT threshold and the correspondent capacity.

Modulation format	Number of cores	Capacity	Units
4-QAM	27	241.92	Tb/s
8-QAM	26	308.67	Tb/s
16-QAM	25	296.8	Tb/s
32-QAM	24	430	Tb/s
64-QAM	23	412.16	Tb/s

As shown in Table 4.6, the highest capacity of 430 Tb/s is achieved with the 32-QAM modulation format with 24 cores in the MCF for a length of 500 km. The SNR for the 4-QAM modulation format and link distance of 500 km, is 24 dB. In Figure 3 a) in [43] for the same value of SNR and link distance the optimal core count is 21. However, for 4-QAM modulation format, Table 4.6 shows that he allowed number of cores is 27. This difference in comparison with [43] is due to the different propagation constant considered which, in our case, produces lower values of the ICXT power.

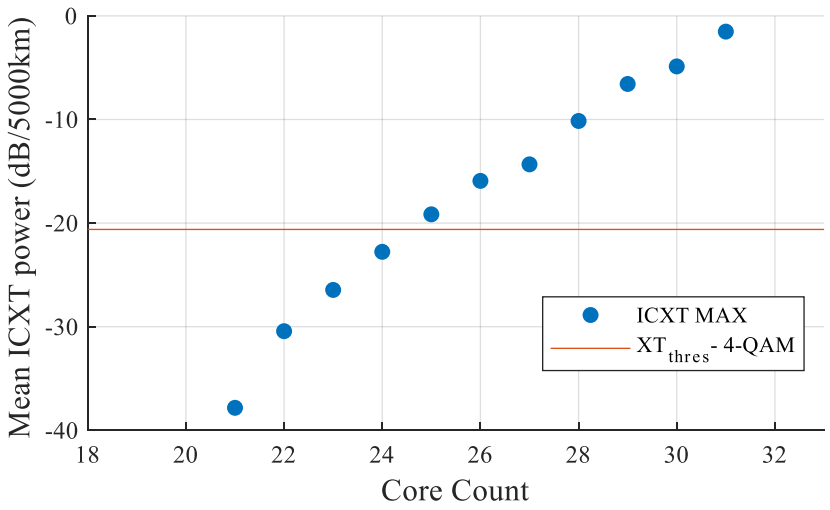

Figure 4.8- Maximum mean ICXT power in dB/5000 km as a function of core count and the crosstalk threshold level for 4-QAM.

The maximum mean of ICXT power in dB/5000 km as a function of core count is represented in Figure 4.8 as well as the ICXT threshold level for 4-QAM shown in Table 4.4. For a fiber length of 5000 km, the only modulation format that accomplished the operating condition given by Equation (4.18), is the 4-QAM, as concluded in section 4.3. As shown in Figure 4.8, the core count must be equal to 24 in order to maximise the total capacity. For a 4-QAM with 24 cores, the total capacity is equal to 215 Tb/s, as shown in Figure 4.4. The value of SNR, for a link distance of 5000 km and 4-QAM modulation format is 14 dB. For this SNR value in [43] Figure 3 a) the optimal core count is 19, as stated before, these differences occur due to the lower values of the mean ICXT power considered in comparison with the ones considered in [43].

4.6 Estimation of the relative mean ICXT power for homogeneous W-profile MCFs

One important issue in MCF transmission is the wavelength dependence of ICXT power over the transmission band. This dependence has not been taken into account in the analysis provided in the previous sections of chapter 4. In order to validate the calculation of the relative mean ICXT power considering the wavelength dependence, which is denominated relative mean ICXT power, the analysis presented in [63] is followed with the goal of obtaining Figure 3 of [63].

The relative mean ICXT power is defined as the ICXT difference between the wavelength λ and the lower wavelength of C band (λ_0) [63]. The relative mean ICXT power, in dB, is given by [63]

$$\Delta ICXT_{dB} = \Delta\lambda \times S \tag{4.21}$$

where $\Delta\lambda = \lambda - \lambda_0$ is the difference between the wavelength λ and the reference wavelength λ_0 and the parameter *S* is the slope of relative mean ICXT power (in dB/nm) for TA-MCFs over the transmission band. The slope of relative mean ICXT power is given by [63]

$$S = \frac{10\log_{10} K}{\Delta\lambda} + 19.85\pi n_1 \sqrt{2\Delta_1}\,\frac{\Lambda_{m,n} + 1.75 A_b w_{tr}}{\lambda\lambda_0} \tag{4.22}$$

where $K = (1 - 0.001256\Delta\lambda)^4$ and A_b is an *b*-dependent coefficient and it is 0.309, 0.607 and 0.867 for *b*=1, 2 and 3, respectively, with $b = |\Delta_2| / \Delta_1$.

The parameters of the TA-MCFs used to validate the calculation of relative mean ICXT power are summarized in Table 4.7.

Table 4.7- Parameters of TA-MCFs for the slope of relative ICXT power calculation.

Parameter	Value	Units
λ_0	1530	nm
$\Lambda_{m,n}$	35, 40, 45	μm
w_{tr}	4.5	μm
n_0	1.444	-
Δ_1	0.35	%
Δ_2	-0.7	%
$b = \lvert\Delta_2\rvert / \Delta_1$	2	-
A_b	0.607	-

The parameters presented in Table 4.7 for TA-MCFs are taken from [63] in order to confirm the results obtained. In Table 4.7, the parameter $\lambda_0 = 1530$ nm is the shortest wavelength of the transmission band (i.e. C+L bands) [63].

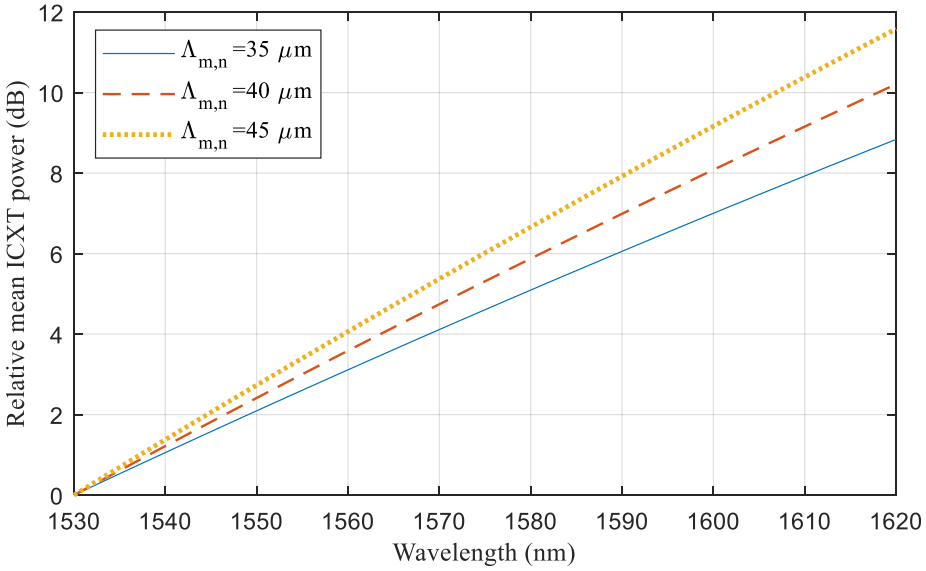

Figure 4.9- Relative mean ICXT power in dB as a function of wavelength in TA-MCFs with the parameters presented in Table 4.7 for distances between closest cores of 35 µm, 40 µm and 45 µm.

The relative mean ICXT power in dB as a function of wavelength in TA-MCFs with the parameters presented in Table 4.7 for distances between closest cores of 35 µm, 40 µm and 45 µm is shown in Figure 4.9. As can be seen from Figure 4.9, the maximum relative mean ICXT power is around 8.8 dB for a distance between cores of 35 µm in TA-MCFs. The results shown in Figure 4.9 are in agreement with Figure 3 of [63]. This allows to conclude that Equation (4.21) is correctly implemented. The distances between closest cores of 45 µm and 35 µm present the higher and the lower values of the relative mean ICXT power, respectively. Hence, the greater the distance between closest cores, the higher is the relative mean ICXT power [63].

Table 4.8 summarizes the parameters of W-profile MCFs used in this work, in order to calculate the relative mean ICXT power and its influence on the total achievable capacity.

Table 4.8- Parameters of the W-profile MCFs considered in this work for the relative mean ICXT power calculation.

Parameter	Value	Units
λ_0	1550	nm
$\Lambda_{m,n}$	[27.9;194]	µm
w_{tr}	6.5	µm
n_0	1.444	-
Δ_1	0.4	%
Δ_2	-0.13	%
$b = \lvert\Delta_2\rvert / \Delta_1$	0.13/0.4=0.3250	-
A_b	0.0864	-

In Table 4.8, the parameter $\Lambda_{m,n}$ is a vector ranging from 27.9 µm to 194 µm which corresponds to the distances between closest cores of a core count between 50 and 2, respectively, for a CD of 260 µm and CT of 33 µm. The parameter λ ranges from λ_0 to 1563.7 nm which corresponds to the nominal frequency of 191.725 THz that has the highest relative ICXT power since it corresponds to the longest wavelength of the transmission band used in this work. The value of parameter A_b is extrapolated for b=0.3250 from the values b=1, 2 and 3 already known (0.309, 0.607 and 0.867, respectively) using spline interpolation.

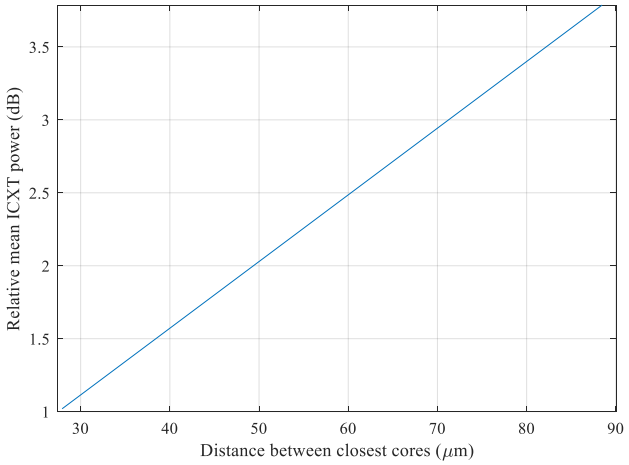

Figure 4.10- Relative mean ICXT power in dB as a function of the distance between closest cores for a W-profile MCF with the parameters presented in Table 4.8 for λ=1563.7 nm.

Figure 4.10 shows the relative mean ICXT power in dB as a function of the distance between closest cores in a W-profile MCF for λ=1563.7 nm. The relative mean ICXT power (in dB) depends linearly on the distance between closest cores [63]. As this distance increases, the relative mean ICXT power (in dB) also increases, as shown in Figure 4.10, and reaches a maximum of 3.85 dB.

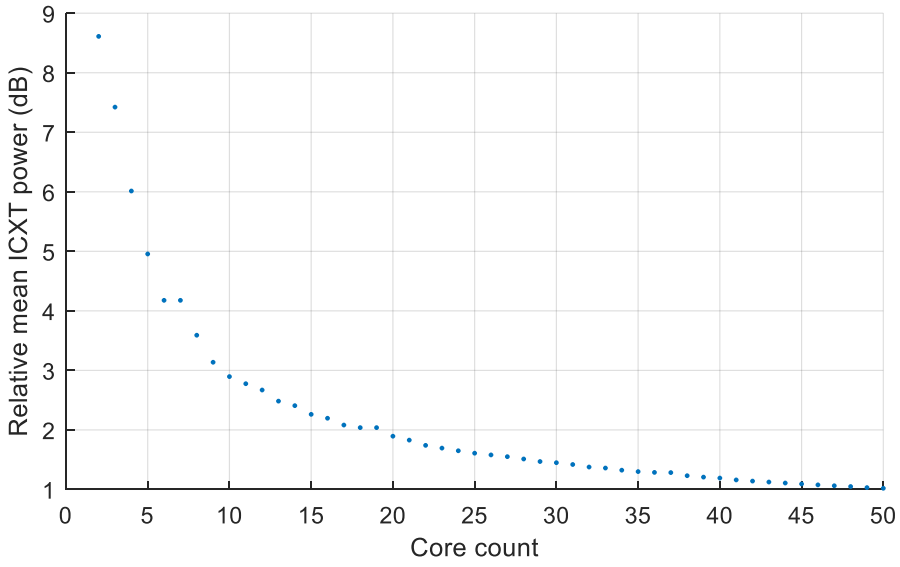

Figure 4.11- Relative mean ICXT power in dB between closest cores as a function of the core count for W-profile MCFs with the parameters presented in Table 4.8.

Figure 4.11 shows the relative mean ICXT power in dB between closest cores as a function of the core count in a W-profile MCF. The minimum distance between two cores of the W-profile MCF d_{min}, for each core count was calculated using Equation (3.6) and the relative mean ICXT power was calculated using Equation (4.21) considering these values of d_{min} for each core count. As expected, the relative mean ICXT power in dB decreases with the increase of the core count. As shown in Figure 4.10, the relative mean ICXT power increases with the cores distance increase. Thus, the relative mean ICXT power is higher for lower core count, as shown in Figure 4.11, due to the fact that lower core counts exhibit higher distances between closest cores.

In order to evaluate the impact of the wavelength dependence of ICXT power over the link it is necessary to add the relative mean ICXT power calculated through Equation (4.21) to the mean ICXT power between two cores calculated through Equation (3.16).

Thus, the mean ICXT power considering the relative mean ICXT power (in dB) in core *m* induced by core *n* is given by

$$\mathrm{x}_{m,n,\Delta ICXT} = x_{m,n} + \Delta ICXT(\lambda = 1563.7) \tag{4.23}$$

where the parameter $\Delta ICXT(\lambda = 1563.7)$ is the relative mean ICXT power (in dB) for a $\lambda = 1563.7$ nm relative to $\lambda_0 = 1550$ nm, for which, the calculations in chapter 3 have been made for.

The total mean ICXT power considering the relative mean ICXT power in core *m,* for $\lambda = 1563.7$ nm, considering the contributions from all the cores of the MCF is given by

$$X_M = \sum_{m \neq n} \mathrm{x}_{m,n,\Delta ICXT} \tag{4.24}$$

4.7 Determination of the total capacity for different link distances considering the relative mean ICXT power

The modulation format and the number of cores that lead to the maximum capacity for the distances of 50 km, 500 km and 5000km, considering the impact of the dependence of the wavelength on the ICXT power are assessed in this section.

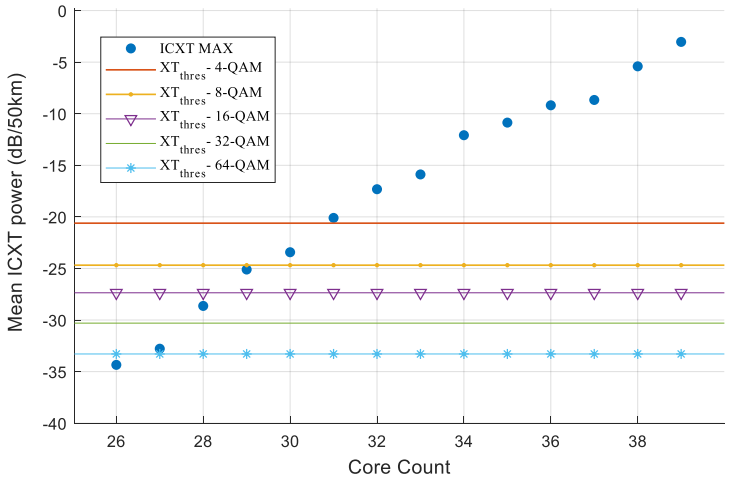

Figure 4.12- Maximum mean ICXT power in dB/50 km considering the relative mean ICXT power as a function of the core count and the ICXT threshold level for different modulation formats.

The maximum mean ICXT power in dB/50 km considering the relative mean ICXT power as a function of the core count is represented in Figure 4.12 as well as the ICXT threshold levels for 4-QAM, 8-QAM, 16-QAM, 32-QAM and 64-QAM modulation formats shown in Table 4.4. The maximum mean ICXT power considering the relative mean ICXT power is calculated through Equation (4.24) with the parameters presented in Table 4.8. Table 4.9 summarizes the achievable number of cores and the corresponding total capacity, for each modulation format, considering that the ICXT threshold has to be higher than the maximum mean ICXT power considering the relative mean ICXT power. The number of cores is extracted from Figure 4.12.

Table 4.9- Allowed number of cores and the corresponding capacity for a WC-MCF for each modulation format for a fiber length of 50 km considering the crosstalk threshold and the relative crosttalk.

Modulation format	Number of cores	Capacity	Units
4-QAM	30	268.8	Tb/s
8-QAM	29	344.28	Tb/s
16-QAM	28	332.41	Tb/s
32-QAM	27	483.84	Tb/s
64-QAM	26	465.92	Tb/s

As expected, the number of allowed cores is reduced and, consequently, the total capacity also decreased in comparison with the results that do not consider the relative mean ICXT power (Table 4.5). The maximum allowed number of cores has decreased one core only for the modulation formats 4-QAM, 8-QAM and 64-QAM. As shown in Table 4.9, the highest capacity of 483.84 Tb/s is achieved by the 32-QAM with 27 cores in the MCF. Hence, considering the relative mean ICXT power, for a length of 50 km, our results indicate that the best modulation format is the 32-QAM.

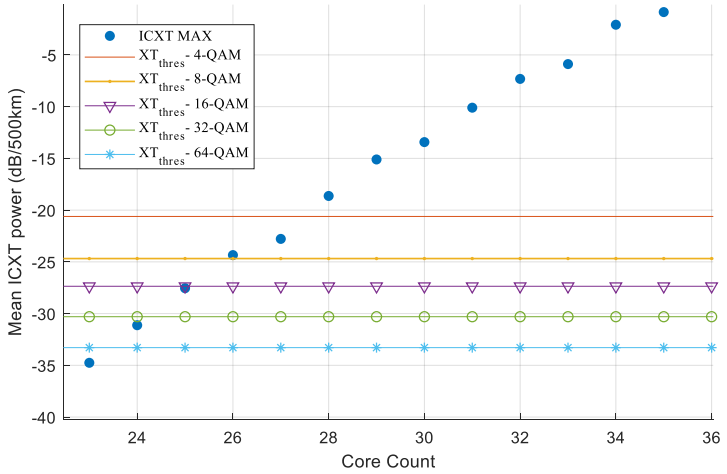

Figure 4.13- Maximum mean ICXT power in dB/500 km considering the relative mean ICXT power as a function of the core count and the ICXT threshold level for different modulation formats.

The maximum mean ICXT power in dB/500 km considering the relative mean ICXT power as a function of the core count is represented in Figure 4.13, as well as the ICXT threshold levels for 4-QAM, 8-QAM, 16-QAM, 32-QAM and 64-QAM modulation formats. Table 4.10 summarizes the maximum allowed number of cores and the corresponding total capacity, for each modulation format, considering that the ICXT threshold has to be higher than the maximum mean ICXT power that take into account the relative mean ICXT power dependence on the wavelength. The number of cores is extracted from Figure 4.13.

Table 4.10- Allowed number of cores and the correspondent capacity for a WC-MCF for each modulation format for a fiber length of 500 km considering the ICXT threshold and the relative ICXT.

Modulation format	Number of cores	Capacity	Units
4-QAM	27	241.92	Tb/s
8-QAM	25	296.8	Tb/s
16-QAM	24	285	Tb/s
32-QAM	24	430	Tb/s
64-QAM	23	412.16	Tb/s

In comparison with the results that do not consider the relative mean ICXT power (Table 4.6), the number of allowed cores has decreased only one core and, consequently, the total capacity also been reduced for the modulation formats 8-QAM and 16-QAM.

Even though, the highest achievable capacity stays the same as when the relative ICXT power is not being considered, i.e., the highest capacity of 430 Tb/s is achieved with 32-QAM and 24 cores in the fiber.

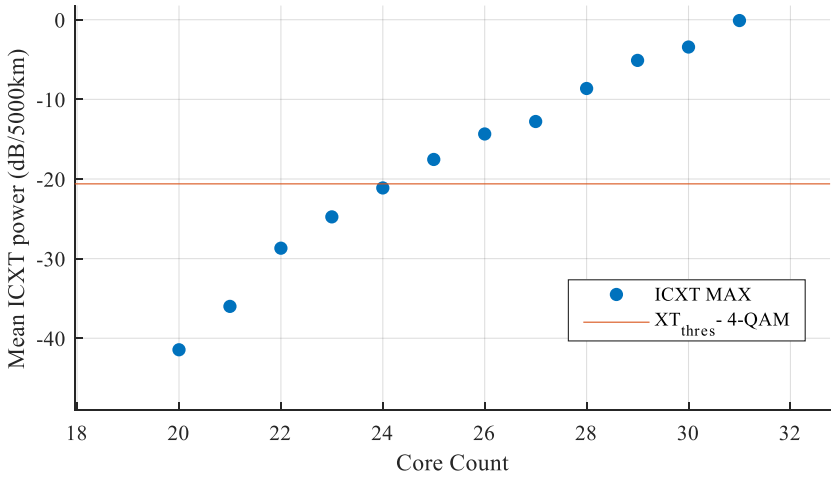

Figure 4.14- Maximum mean ICXT power in dB/5000 km considering the relative mean ICXT power as a function of the core count and the ICXT threshold level for 4-QAM.

The maximum mean ICXT power in dB/5000 km considering the relative mean ICXT power as a function of the core count as well as the ICXT threshold level for the 4-QAM format is represented in Figure 4.14. The maximum mean ICXT power considering the relative mean ICXT power is calculated through Equation (4.23) with the parameters presented in Table 4.8. For a fiber length of 5000 km, as previously shown, the only modulation format that accomplishes the operating condition given by Equation (4.18) is the 4-QAM. As shown in Figure 4.14, the core count must be equal to 23 in order to maximise the total link capacity. For a 4-QAM with 23 cores, the total capacity is equal to 206.08 Tb/s. Figure 4.14 shows a decrease of one, core which represents a total capacity reduction around 8.9 Tb/s, in comparison with the results that do not consider the relative mean ICXT power shown in Figure 4.8.

4.8 OSNR, link reach and capacity in presence of nonlinear interference noise

In uncompensated coherent systems, due to the large dispersion accumulated along transmission, large signal decorrelation occurs during propagation which is recorrelated at the receiver by the electronic dispersion compensation. At the same time, electronic dispersion compensation decorrelates non-linear effects, "averaging" the non-linear effects contributions [64]. Due to this averaging, NLI can be modelled as excess additive Gaussian noise, at least for low-to-moderate NLI, even in the absence of added ASE noise in the link [49, 50]. This assumption on NLI noise is valid only when the non-linearity has a "mild" effect on the link performance [50]. Considering this, the system performance can be evaluated by correcting the OSNR that reaches the optical receiver. The modified OSNR, also so called non-linear OSNR, in linear units, is given by [64]

$$osnr_{modified} = \frac{P}{p_{n,ASE} + p_{NLI}} \tag{4.25}$$

where P is the average signal power at fiber input per polarization for channel t, $p_{n,ASE}$ is the power of ASE noise given by Equation (4.16) in which is calculated at the bandwidth of the signal t , Δf_t, and per polarization (i.e divided for 2) and p_{NLI} is the NLI power. The p_{NLI} for channel t can be written as [64]

$$p_{NLI}\left(f_t\right) \approx \int_{f_t - R_s/2}^{f_t + R_s/2} G_{NLI}\left(f\right) df \approx G_{NLI}\left(f_t\right) R_s \tag{4.26}$$

where f_t is the central frequency of channel t, the symbol rate, R_s, is given by Equation (4.2) and $G_{NLI}\left(f_t\right)$ is the PSD of NLI noise of channel t over multiple fiber spans given by [64]

$$G_{NLI}\left(f_t\right) = N_{spans}\left[G_{SCI}^{lspan}\left(f_t\right) + G_{XCI}^{lspan}\left(f_t\right)\right] \tag{4.27}$$

where N_{spans} is the number of spans of the link, $G_{SCI}^{lspan}\left(f_t\right)$ is the PSD of self-channel interference (SCI) of channel t over a span, which is the interference caused by channel t on itself and $G_{XCI}^{lspan}\left(f_t\right)$ is the PSD of cross-channel interference (XCI) of channel t over

a span, which is the interference caused by other channels on channel *t*. The PSD of SCI of channel *t*, $G_{SCI}^{lspan}\left(f_t\right)$, is given by [64]

$$G_{SCI}^{lspan}\left(f_t\right)=G_t^3\frac{3\gamma^2}{2\pi\alpha\left|\beta_2\right|}\operatorname{arcsinh}\left(\frac{\pi^2\left|\beta_2\right|}{2\alpha}\Delta f_t^2\right) \tag{4.28}$$

where $G_t=P/\Delta f_t$ is the signal PSD of channel *t* per polarization, Δf_t is the bandwidth of channel *t*, which for Nyquist spectrum shaping is equal to R_s, γ is the fiber nonlinearity coefficient, in this work set as 1.3 $W^{-1}km^{-1}$ [49] and β_2 is the chromatic dispersion given by $\beta_2=-\lambda_0 D_{\lambda_0}/\left(2\pi c\right)$, in which λ_0 corresponds to the wavelength of the central frequency of the WDM signal and D_{λ_0} is the fiber dispersion parameter equal to 16 ps/nm/km [49].

The PSD of XCI of channel *t*, $G_{XCI}^{lspan}\left(f_t\right)$, is given by [64]

$$G_{XCI}^{lspan}\left(f_t\right)=G_t\frac{3\gamma^2}{2\pi\alpha\left|\beta_2\right|}\sum_{\substack{t'=1\\ t'\neq t}}^{N_{ch}}G_{t'}^2\ln\left(\frac{f_{tt'}+\Delta f_{t'}/2}{f_{tt'}-\Delta f_{t'}/2}\right) \tag{4.29}$$

where N_{ch} is the number of WDM channels and is given by Equation (4.5) and $f_{tt'}=\left|f_t-f_{t'}\right|$.

The power that maximizes the modified OSNR, i.e., the optimal launch power, p_{ch}, is given by [64]

$$p_{ch}=\sqrt[3]{\frac{p_{n,ASE}}{2\eta}} \tag{4.30}$$

Where $\eta=p_{NLI}/\left(P\right)^3$, is a parameter that is specific for a particular fiber link. The modified OSNR, in linear units, which considers the optimal launch power is given by [64]

$$osnr_{modified}=\frac{p_{ch}}{p_{n,ASE}+\eta p_{ch}^3} \tag{4.31}$$

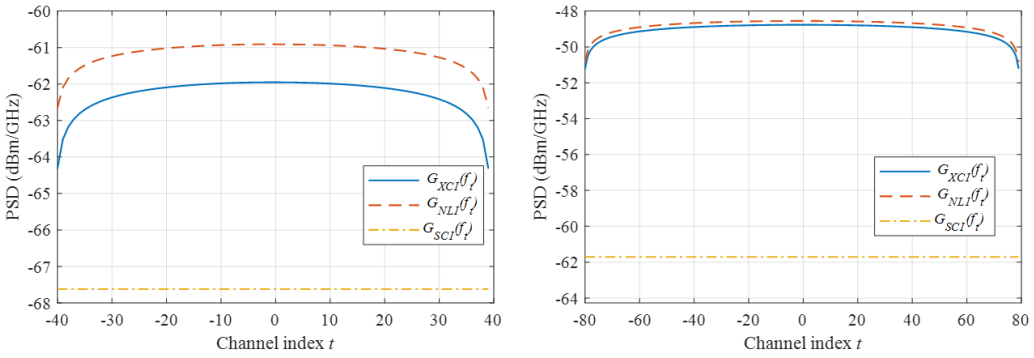

Figure 4.15- The PSD of NLI, XCI and SCI as a function of channel index for a) 4-QAM and b) 64-QAM modulation formats

Figure 4.15 shows the PSD of NLI, XCI and SCI as a function of channel index for a) 4-QAM and b) 64-QAM modulation formats. The PSD of NLI, XCI and SCI was calculated according to Equations (4.27), (4.28), (4.29), respectively. The average signal power P considered for each channel t was 0.3 mW. The nominal central frequencies considered in this work for the 4-QAM and 64-QAM modulation format are summarized in Appendix B. The 80 WDM channels for the 4-QAM modulation format have a 50 GHz channel width. For the case of 64-QAM modulation format, 160 WDM channels with 25 GHz spacing were considered. The zero channel index represents the WDM central channel considered for each modulation format. As shown in Figure 4.15, the central channel represents the worst-case scenario, i.e., has a higher value of $G_{NLI}(f_t)$, as expected [64]. As shown in Figure 4.15 b), the 64-QAM modulation format has a higher value of NLI than the 4-QAM modulation format in Figure 4.15 a).

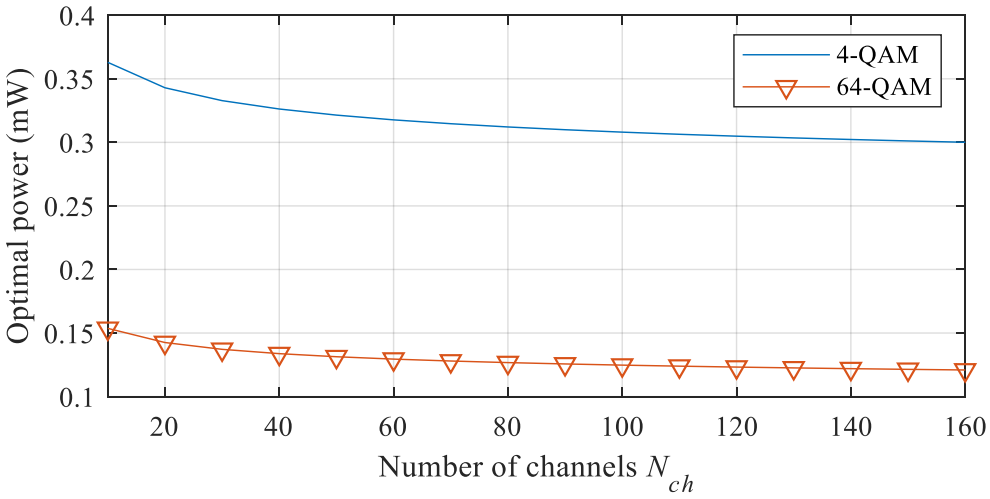

Figure 4.16- Optimal channel launch power as a function of the number of WDM channels for a link distance of 50 km for 4-QAM and 64-QAM, for the WDM central channel.

The optimal launch power for the two signal polarizations as a function of the number of WDM channels for 4-QAM and 64-QAM modulation formats and a link distance of 50 km is plotted in Figure 4.16. The optimal channel power was calculated using Equation (4.30) and the WDM frequency grids are the ones considered in Appendix B. The optimal power decreases with the increase of the number of WDM channels as shown in Figure 4.16. However, the optimal channel power remains practically the same for a number of channels above 100, the decrease of the optimal power is not much significant, which means that from this point onwards the channels added to the system do not have a significant impact in central channel. That means that the 100 channels near the central channel have greater preponderance in NLI power. The modulation formats 4-QAM and 64-QAM show practically the same behaviour for the optimal launch power as the number of channels increase. However, the 64-QAM modulation format presents lower values of the optimal launch power as expected due to the different channel width considered [50]. The optimal power decreases with the increase of the modulation format due to the more significant NLI in the fiber (as shown in Figure 4.15) and in order to decrease this effect, the optimal launch power is decreased.

In order to compute the modified OSNR, the optimal launch power was calculated using Equation (4.30). The optimal launch power was calculated for the central channel which represents the worst-case scenario, i.e., has a higher contribution of $G_{XCI}^{lspan}\left(f_t\right)$ as

shown in Figure 4.15. The optimal channel power and the value of parameter η obtained for each modulation format are summarized in Table 4.11 and are independent of the number of fiber sections considered [64].

Table 4.11- Optimal power for the two signal polarizations for each modulation format and the value of parameter η.

Modulation format	Optimal power [mW]	η
4-QAM	0.312	6.72×10^{3}
8-QAM	0.218	1.29×10^{4}
16-QAM	0.182	1.67×10^{4}
32-QAM	0.136	3.24×10^{4}
64 QAM	0.120	3.85×10^{4}

The modified OSNR was calculated using Equation (4.31) for the optimal launch power and its values are summarized in Table 4.12.

Table 4.12- Modified OSNR, in dB, for each modulation format and for the link distances of 50, 500 and 5000 km.

Modulation Format	L_{tot}=50 km	L_{tot}=500 km	L_{tot}=5000 km	Units
4-QAM	33.0862	23.0862	13.0862	dB
8-QAM	33.3075	23.3075	13.3075	dB
16-QAM	33.7684	23.7684	13.7684	dB
32-QAM	33.4592	23.4592	13.4592	dB
64-QAM	33.7383	23.7383	13.7383	dB

The modified OSNR decreases with the increase of the total distance of the link, as shown in Table 4.12, due to the increase of the total power of ASE noise, since longest link distances have more spans. The values of the required OSNR under ideal and real conditions, in dB, for each modulation format are summarized in Table 4.13

Table 4.13- Required OSNR under ideal and real conditions in dB for each modulation format.

Modulation Format	$OSNR_{req,i}$ [dB]	$OSNR_{req}$ [dB]
4-QAM	8.53	12.53
8-QAM	12.60	16.60
16-QAM	15.19	19.19
32-QAM	18.22	22.22
64-QAM	21.12	25.12

Since the bandwidth considered for calculation of the p_{NLI} is equivalent to the symbol rate, the required OSNR was recalculated using Equation (4.8), but considering the symbol rate of each modulation format instead of the reference bandwidth B_{ref}. The required OSNR under real conditions was calculated using Equation (4.14). These values are shown in Table 4.13.

Through the analyses of the Table 4.12 and 4.13, it is possible to conclude that for a link distance of 50 km, every modulation format can be used since the operating condition presented in Equation (4.18) is always accomplished. For a link distance of 500 km, the 64-QAM modulation format should be excluded, since it does not satisfy the operating condition. In the absence of NLI, the 64-QAM format was able to accomplish the operating condition for the 500 km distance, as described in section 4.2. For a link distance of 5000 km, only the modulation 4-QAM can be used.

Since the bandwidth considered for the calculation of the p_{NLI} is equivalent to the symbol rate, the threshold level was again calculated. The ICXT level, in decibel, for a maximum allowed OSNR penalty considering that the bandwidth of the channel is equal to the symbol rate, is given by

$$XT(\Delta OSNR) = 10\log_{10}\left(1 - \frac{1}{10^{\frac{\Delta OSNR}{10}}}\right) - OSNR_{req,i} \tag{4.32}$$

where the values of $OSNR_{req,i}$ are summarized in table 4.13. The ICXT threshold level is given by Equation (4.20). The values of the recalculated ICXT threshold levels are summarized in Table 4.14.

Table 4.14- ICXT threshold levels, in dB, for different modulation format considering the bandwidth of the channel equal to the symbol rate

Modulation format	$XT_{\mu,thres}$ [dB]
4-QAM	-20.7
8-QAM	-24.77
16-QAM	-27.36
32-QAM	-30.39
64-QAM	-33.29

The values presented in Table 4.14 are equal to the values presented in Table 4.4, as expected. Since in Equation (4.32) the term $10\log_{10}\left(\frac{R_s}{B_{ref}}\right)$ was withdraw which converts the OSNR of the reference bandwidth in the OSNR of the signal.

Since for a link distance of 50 km, all the modulation formats can be used, the reached capacities are the same as the ones found in the absence of NLI (Figure 4.6 and Figure 4.12, including the wavelength dependence of the ICXT power over the transmission band). So, for a length of 50 km, our results indicate that the best modulation format is the 32-QAM since it reaches the highest capacity of 483.84 Tb/s with 27 cores in the fiber.

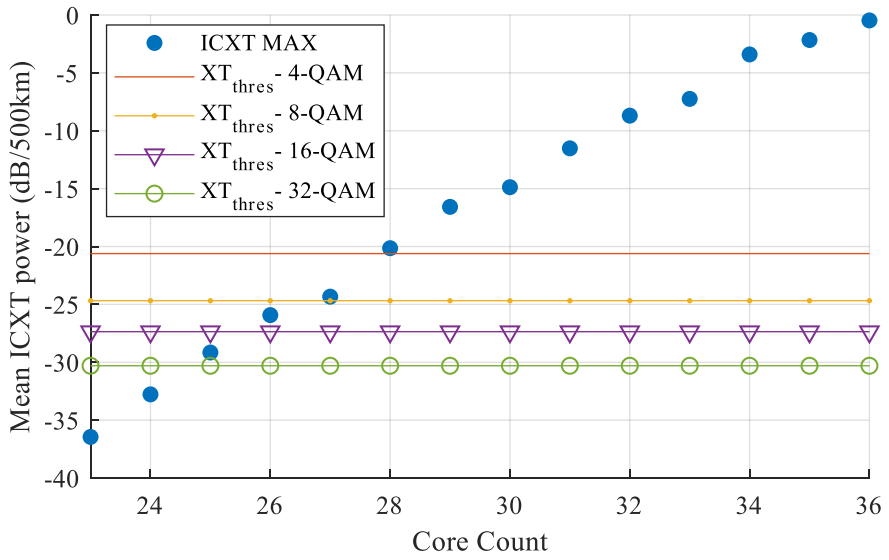

Figure 4.17- Maximum mean ICXT power in dB/500 km as a function of core count and the ICXT threshold level for different modulation formats considering the NLI.

Figure 4.17 presents the maximum mean ICXT power in dB/500 km as a function of core count for the modulation formats that accomplish the condition presented in Equation (4.18). The number of allowed cores in the fiber extracted from Figure 4.17 is the same that in the case when the NLI is not being considered (as shown in Figure 4.7). The best modulation format is the 32-QAM since it reaches the highest capacity of 430 Tb/s with the 32-QAM with 24 cores. Although the modulation format 64-QAM does not comply with the required OSNR, the total capacity is the same as when the NLI is not being considered. Figure 4.17 do not consider the wavelength dependence of ICXT power over the transmission band.

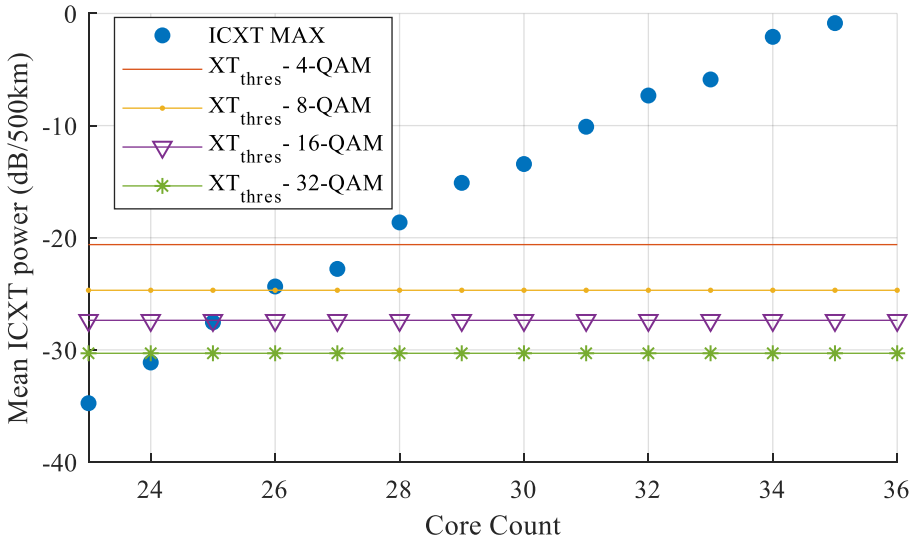

Figure 4.18-Maximum mean ICXT power in dB/500 km considering the relative mean ICXT power and the presence of the NLI as a function of the core count and the ICXT threshold level for different modulation formats.

Figure 4.18 considers the relative mean ICXT power and the presence of the NLI. Figure 4.18 presents the maximum mean ICXT power in dB/ 500 km as a function of the core count for the modulation formats that accomplish the condition presented in Equation 4.18. The number of the allowed cores for the modulation formats that accomplish the condition presented in Figure 4.18 are the same that the ones presented in Figure 4.13, where the NLI is absent. So, the highest capacity of 430 Tb/s is achieved with the 32-QAM modulation format with 24 cores in the fiber when the NLI and the wavelength dependence of ICXT power are being considered.

For a link distance of 5000 km, the total capacity is also the same that when the NLI is not being considered (Figure 4.8), since there are no changes in the allowed modulation format. So, the total capacity of 215 Tb/s is achieved by the 4-QAM modulation format with 24 cores in the fiber. Considering both the presence of the NLI and the wavelength dependence of the ICXT power over the transmission band, the total capacity of 206.08 Tb/s is achieved with 23 cores in the fiber, and this result is the same that the one presented in Figure 4.14.

4.9 Conclusions

In this chapter, the total capacity was assessed for different modulation formats for coherent detection optical communication systems that use flexible grid over the C-band. Firstly, considering only the bandwidth limitation of the C-band, the results obtained show that the maximum total capacity of 900 Tb/s is achieved for a core count of 50 with the modulation formats 32-QAM and 64-QAM.

In order to consider the ICXT impairment in the link, the best modulation format for metro or access networks, regional networks and long-distance networks was assessed, considering the required OSNR under real conditions and the OSNR that reaches the optical receiver input. For our parameters, all the modulation formats can be used for metro and regional networks, whereas for long-distance networks, only the 4-QAM can be used.

The ICXT threshold level corresponding to the outage probability of 10^{-5} was calculated for each modulation formats considered, and the total capacity of the link was maximised based on the designed threshold levels. We have found that for metro or access networks (50 km) with a W-profile with 27 cores, a capacity of 483.84 Tb/s is achieved by 32-QAM and the maximum mean ICXT power is -34.5 dB. For regional networks (500 km), the total capacity of 430 Tb/s is achieved by 32-QAM with 24 cores in the W-profile fiber and the maximum mean ICXT power of -32.75 dB. Finally, for long-distance networks (5000 km), the capacity achieved for a 4-QAM is around 215 Tb/s with 24 cores in the MCF and the maximum mean ICXT power of -22.75 dB.

One of the impairments in MCF transmission assessed in this chapter was the wavelength dependence of ICXT power over the transmission band. This dependence was calculated and validated by the works in the literature and the impact on the link was studied. Our results indicate that the relative mean ICXT power decreases with the increase of the core count. For 50 km links, the capacity was decreased for the modulation formats 4-QAM, 8-QAM and 64-QAM, but the highest capacity of 483.84 Tb/s is still the same than when this effect is not being considered. It is achieved using 32-QAM with 27 cores in the MCF. For the distance of 500 km, the relative mean ICXT power decreases the total capacity for the modulation formats 8-QAM and 16-QAM. The highest capacity of 430 Tb/s is achieved with 32-QAM and 24 cores in the fiber. For a link

distance of 5000 km, the relative mean ICXT power decrease the number of allowed cores to 23, which represents a decrease of 8.9 Tb/s in the total capacity of 206.08 Tb/s with 4-QAM modulation format.

Finally, in order to consider the NLI impairment, the OSNR that reaches the optical receiver was corrected and the optimal launch power was calculated for each modulation format. Our results have shown that for a link distance of 500 km, the 64-QAM modulation format could not be used. Otherwise, in terms of the total highest capacity of the link, the results obtained are equivalent to the ones obtained when the NLI is not being considered.

Chapter 5

Conclusions and future work

In this chapter, the main final conclusions achieved in this work are presented as well as some suggestions for future work.

5.1 Final conclusions

In Chapter 2, the different types of MCFs that allow the SDM approach as a promising solution to increase the capacity per cross-sectional were described. The ICXT power as an impairment of the SDM networks was presented. The flexible grid and coherent optical communications were also described as a way to achieve higher bit rate in optical transmission.

Chapter 3 described the method used to obtain the optimum core layout for different number of cores which maximises the distance between two neighbour cores presented in [59], since the core layout design is similar to the well-known problem of packing circles in a circle in order to reduce the mean ICXT power. The mean ICXT power was calculated for a TA-MCF in order to validate the equations implemented in MATLAB and a good agreement was achieved. To estimate the mean ICXT power for a W-profile MCF, the methodology used was changed to correspond to the structure of the W-profile MCF. Furthermore, a study was accomplished in order to assess the impact of the propagation constant on the mean ICXT power. Our results show that the mean ICXT

power is very sensitive to the slight variations of the value of the propagation constant. An increase of 0.0203% of the propagation constant produces a variation on the mean ICXT power of 7 dB and 13 dB for a distance between neighbour cores of 30 μm and 45μm, respectively.

Chapter 4 assessed the total capacity of the system considering different impairments in the transmission such as the bandwidth limitation of the C-band, the ICXT power and its wavelength dependence over the transmission band and the NLI effect. Our results indicate that for a metro access network (represented with a link distance of 50 km) supported by a W-profile MCF with 27 cores the capacity of 483.84 Tb/s is achieved by the 32-QAM modulation format considering the wavelength dependence and the NLI effect. For regional networks (represented with a link distance of 500 km), the highest capacity of 430 Tb/s is achieved with 32-QAM and 24 cores in the fiber. Finally, for long-distance networks (represented with a link distance of 5000 km), the total capacity of 206.08 Tb/s is achieved with 23 cores with 4-QAM modulation format.

5.2 Future work

SDM is a promising technology to overcome the capacity crush; however, there are many requirements that should be deeply investigated in order to make SDM with WC-MCF a reliable solution. Additional studies are needed to justify the benefits and establish the requirements for different types of network relating with the different solutions given by SDM. With that in mind some future work proposals are presented:

- Optimization of the core layout and estimation of the ICXT level for W-profile MCFs with cladding diameter compatible with the standard SM-SCF diameter of 125 μm;
- Analysis of the total capacity and maximum link reach for several QAM modulation formats, for networks supported by W-profile MCFs with 125 μm cladding diameter;
- Estimation of the ICXT level, and analysis of the total capacity and maximum link reach for networks with TA-MCFs proposed in the literature;

- Estimation of the ICXT level, and analysis of the total capacity and maximum link reach for networks with TA-MCFs with 125 μm cladding diameter.

References

[1] "Cisco visual networking index: forecast and methodology, 2016–2021, " Cisco White Paper [Online], Available: https://www.cisco.com/c/en/us/solutions/collateral/service-provider/visual-networking-index-vni/complete-white-paper-c11-481360.pdf.

[2] K. Saitoh and S. Matsuo, "Multicore fiber technology," *Journal of Lightwave Technology,* vol. 34, no. 1, pp. 55-66, Jan. 1, 2016, doi: 10.1109/Jlt.2015.2466444.

[3] A. Sano, T. Kobayashi, S. Yamanaka, A. Matsuura, H. Kawakami, Y. Miyamoto, K. Ishihara, and H. Masuda, "102.3-Tb/s (224 x 548-Gb/s) C- and extended L-band all-Raman transmission over 240 km using PDM-64QAM single carrier FDM with digital pilot tone," in Optical Fiber Communication Conference/National Fiber Optic Engineers Conference (OFC/NFOEC), Los Angeles, CA, USA, Mar. 2012, Paper PDP5C.3.

[4] D. Richardson, J. Fini, and L. Nelson, "Space-division multiplexing in optical fibres," *Nature Photonics,* vol. 7, no. 5, pp. 354-362, May 2013, doi: 10.1038/nphoton.2013.94.

[5] T. Morioka, "New generation optical infrastructure technologies: "EXAT initiative" towards 2020 and beyond," in 2009 14th OptoElectronics and Communications Conference (OECC), Hong Kong, China, Jul. 2009, Paper FT4.

[6] T. Mizuno, H. Takara, K. Shibahara, A. Sano, and Y. Miyamoto, "Dense space division multiplexed transmission over multicore and multimode fiber for long-haul transport systems," *Journal of Lightwave Technology,* vol. 34, no. 6, pp. 1484-1493, Mar. 15, 2016, doi: 10.1109/jlt.2016.2524546.

[7] I. Morita, K. Igarashi, H. Takahashi, T. Tsuritani, and M. Suzuki, "Trans-oceanic class ultra-long-haul transmission using multi-core fiber," *Optics Express,* vol. 22, no. 26, pp. 31761-31773, Dec. 2014, doi: 10.1364/oe.22.031761.

[8] T. Mizuno, H. Takara, A. Sano, and Y. Miyamoto, "Dense space division multiplexed transmission over multi-core and multi-mode fiber," in 2015 Optical Fiber Communications Conference and Exhibition (OFC), Los Angeles, CA, USA Mar. 2015, Paper Th1D.2.

[9] F. Lobato, A. Jacob, J. Rodrigues, A. Cartaxo, and J. Costa, "Inter-core crosstalk aware greedy algorithm for spectrum and core assignment in space division multiplexed elastic optical networks," *Optical Switching and Networking,* vol. 33, pp. 61-73, Jul. 2019, doi: 10.1016/j.osn.2019.03.003.

[10] J. M. Galve, I. Gasulla, S. Sales, and J. Capmany, "Fronthaul design for radio access networks using multicore fibers," *Waves Magaz.,* vol. 7, no. 1, pp. 69-80, 2015.

[11] Z. Feng, L. Xu, Q. Wu, M. Tang, S. Fu, W. Tong, P. P. Shum, and D. Liu, "Ultra-high capacity WDM-SDM optical access network with self-homodyne detection downstream and 32QAM-FBMC upstream," *Optics Express,* vol. 25, no. 6, pp. 5951-5961, Mar. 2017, doi: 10.1364/OE.25.005951.

[12] R. Lin, J. V. Kerrebrouck, X. Pang, M. Verplaetse, O. Ozolins, A. Udalcovs, L. Zhang, L. Gan, M. Tang, S. Fu, R. Schatz, U. Westergren, S. Popov, D. Liu, W. Tong, T. D. Keulenaer, G. Torfs, J. Bauwelinck, X. Yin, and J. Chen, "Real-time 100 Gbps/λ/core NRZ and EDB IM/DD transmission over multicore fiber for

intra-datacenter communication networks " *Optics Express,* vol. 26, no. 8, pp. 10519-10526, Apr. 2018.

[13] F. Moreno-Muro, R. Rumipamba-Zambrano, P. Pavón-Marino, J. Perelló, J. Gené, and S. Spadaro, "Evaluation of core-continuity-constrained ROADMs for flex-grid/MCF optical networks," *IEEE/OSA Journal of Optical Communications and Networking,* vol. 9, no. 11, pp. 1041-1050, Nov. 2017, doi: 10.1364/JOCN.9.001041.

[14] B. Puttnam, R. Luís, E. Agrell, G. Rademacher, J. Sakaguchi, W. Klaus, G. Saridis, Y. Awaji, and N. Wada, "High capacity transmission systems using homogeneous multi-core fibers," *Journal of Lightwave Technology,* vol. 35, no. 6, pp. 1157-1167, Mar. 15, 2017, doi: 10.1109/jlt.2017.2669207.

[15] G. Saridis, D. Alexandropoulos, G. Zervas, and D. Simeonidou, "Survey and evaluation of space division multiplexing: from technologies to optical networks," *IEEE Communications Surveys & Tutorials,* vol. 17, no. 4, pp. 2136 - 2156, Aug. 2015, doi: 10.1109/COMST.2015.2466458.

[16] D. Kumar and R. Ranjan, "Estimation of crosstalk in homogeneous multicore fiber for high core count under limited cladding diameter," in 2017 Conference on Information and Communication Technology (CICT), Gwalior, India, Nov. 2017.

[17] K. Takenaga, Y. Arakawa, S. Tanigawa, N. Guan, S. Matsuo, K. Saitoh, and M. Koshiba, "Reduction of crosstalk by trench-assisted multi-core fibre," in 2011 Optical Fiber Communication Conference and Exposition and the National Fiber Optic Engineers Conference, Los Angeles, USA March 2011, Paper OWJ4.

[18] A. Sano, H. Takara, T. Kobayashi, and Y. Miyamoto, "Crosstalk-managed high capacity long haul multicore fiber transmission with propagation-direction interleaving," *Journal of Lightwave Technology,* vol. 32, no. 16, pp. 2771-2779, Aug. 15, 2014, doi: 10.1109/JLT.2014.2320826.

[19] T. Hayashi, T. Taru, O. Shimakawa, T. Sasaki, and E. Sasaoka, "Design and fabrication of ultra-low crosstalk and low-loss multi-core fiber," *Optics Express,* vol. 19, no. 17, pp. 16576-16592, Aug. 2011, doi: 10.1364/OE.19.016576.

[20] Y. Goto, K. Nakajima, T. Matsui, T. Kurashima, and F. Yamamoto, "Influence of cladding thickness on transmission loss and its relationship with multicore fiber structure," *Journal of Lightwave Technology,* vol. 33, no. 23, pp. 4942 - 4949, Dec. 1 2015, doi: JLT.2015.2493372.

[21] T. Hayashi and T. Nakanishi, "Multi-core optical fibers for the next-generation communications," *SEI Technical Review,* no. 86, pp. 23-28, Apr. 2018 2018.

[22] D. Qian, M.-F. Huang, E. Ip, Y. K. Huang, Y. Shao, J. Hu, and T. Wang, "101.7-Tb/s (370x294-Gb/s) PDM-128QAM-OFDM transmission over 3x55-km SSMF using pilot-based phase noise mitigation," in IEEE/OSA Optical Fiber Communication Conference (OFC), Los Angeles, CA, USA, Mar. 2011, Paper PDPB5.

[23] Y. Awaji, "Review of space-division multiplexing technologies in optical communications," *IEICE Transactions on Communications,* vol. E102–B,, no. 1, pp. 1-16, Jan. 2019, doi: 10.1587/transcom.2017EBI0002.

[24] J. Sakaguchi, Y. Awaji, N. Wada, A. Kanno, T. Kawanishi, T. Hayashi, T. Taru, T. Kobayashi, and M. Watanabe, "109-Tb/s (7×97×172-Gb/s SDM/WDM/PDM) QPSK transmission through 16.8-km homogeneous multi-core fiber," in 2011 Optical Fiber Communication Conference and Exposition and the National Fiber Optic Engineers Conference, Los Angeles, CA, USA, Mar. 2011, Paper PDPB6.

[25] B. Zhu, T. Taunay, M. Fishteyn, X. Liu, S. Chandrasekhar, M. Yan, J. M. Fini, E. Monberg, and F. Dimarcello, "112-Tb/s Space-division multiplexed DWDM

transmission with 14-b/s/Hz aggregate spectral efficiency over a 76.8-km seven-core fiber " *Optics Express,* vol. 19, no. 17, pp. 16665-16671, Aug. 2011, doi: 10.1364/OE.19.016665.

[26] J. Sakaguchi, J. Puttnam, W. Klaus, YoshinariAwaji, N. Wada, A. Kanno, T. Kawanishi, K. Imamura, H. Inaba, K. Mukasa, R. Sugizaki, T. Kobayashi, and M. Watanabe, "305 Tb/s space division multiplexed transmission using homogeneous 19-core fiber," *Journal of Lightwave Technology,* vol. 31, no. 4, Feb. 15, doi: 10.1109/JLT.2012.2217373.

[27] A. Turukhin, O. Sinkin, H. G. Batshon, Y. Sun, M. Mazurczyk, C. R. Davidson, J.-X. Cai, M. Bolshtyansky, D. Foursa, and A. Pilipetskii, "High capacity ultralong-haul power efficient transmission using 12-Core fiber," *Journal of Lightwave Technology,* vol. 35, no. 4, Feb. 15 2017, doi: 10.1109/JLT.2016.2599021.

[28] A. Turukhin, H. G. Batshon, M. Mazurczyk, Y. Sun, C. R. Davidson, J.-X. Chai, O. V. Sinkin, W. Patterson, G. Wolter, M. A. Bolshtyansky, D. G. Foursa, and A. Pilipetskii, "Demonstration of 0.52 Pb/s potential transmission capacity over 8,830 km using multicore fiber," in 42nd European Conference on Optical Communication (ECOC), Dusseldorf, Germany, Sep. 2016.

[29] S. Korotky, "Price-points for components of multi-core fiber communication systems in backbone optical networks," *IEEE/OSA Journal of Optical Communications and Networking* vol. 4, no. 5, pp. 426 - 435, May 2012, doi: 10.1364/JOCN.4.000426.

[30] H. Ono, K. Takenaga, K. Ichii, and M. Yamada, "Amplification technology for multi-core fiber transmission," in 2014 IEEE Photonics Society Summer Topical Meeting Series, Montreal, QC, Canada, Jul. 2014 2014, Paper SUM.2014.82.

[31] K. Igarashi, K. Takeshima, T. Tsuritani, H. Takahashi, S. Sumita, I. Morita, Y. Tsuchida, M. Tadakuma, K. Maeda, T. Saito, K. Watanabe, K. Imamura, R. Sugizaki, and M. Suzuki, "110.9-Tbit/s SDM transmission over 6,370 km using a full C-band seven-core EDFA " *Optics Express,* vol. 21, no. 15, pp. 18053-18060, Jul. 2013, doi: 10.1364/OE.21.018053.

[32] K. Saitoh and S. Matsuo, "Multicore fibers for large capacity transmission," *Nanophotonics,* vol. 2, no. 5-6, pp. 441-459, Nov. 2013, doi: 10.1515/nanoph-2013-003.

[33] K. Nakajima, T. Matsui, K. Saito, T. Sakamoto, and N. Araki, "Multi-Core fiber technology: next generation optical communication strategy," *IEEE Communications Standards Magazine,* vol. 1, no. 3, pp. 38-45, Sep. 2017, doi: 10.1109/MCOMSTD.2017.1700017.

[34] W. Klaus, B. Puttnam, R. Luis, J. Sakaguchi, J. Mendinueta, Y. Awaji, and N. Wada, "Advanced space division multiplexing technologies for optical networks [invited]," *IEEE/OSA Journal of Optical Communications and Networking,* vol. 9, no. 4, pp. C1-C11, Apr. 2017, doi: 10.1364/jocn.9.0000c1.

[35] L. Gan, J. Zhou, S. Fu, M. Tang, and D. Liu, "Efficient channel model for homogeneous weakly coupled multicore fibers," *IEEE Journal of Selected Topics in Quantum Electronics,* vol. 26, no. 4, pp. 1-9, May 2019, doi: 10.1109/JSTQE.2019.2916423.

[36] B. Puttnam, R. Luís, W. Klaus, J. Sakaguchi, J. Mendinueta, Y. Awaji, N. Wada, Y. Tamura, T. Hayashi, M. Hirano, and J. Marciante, "2.15 Pb/s transmission using a 22 core homogeneous single-mode multi-core fiber and wideband optical comb," in 2015 European Conference on Optical Communication (ECOC), Valencia, Spain, Sept. 2015, Paper PDP3.1.

[37] T. Sakamoto, T. Matsui, K. Saitoh, S. Saitoh, K. Takenaga, and T. M. e. all, "Low-loss and low-DMD 6-Mode 19-Core fiber with cladding diameter of less than 250 μm," *Journal of Lightwave Technology,* vol. 35, no. 3, Feb. 1 2017, doi: 10.1109/JLT.2016.2610479.

[38] S. Kawakami and S. Nishida, "Characteristics of a doubly clad optical fiber with a low-index inner cladding," *IEEE Journal of Quantum Electronics,* vol. 10, no. 12, pp. 879-887, Dec. 1974, doi: 10.1109/JQE.1974.1068118.

[39] T. Nakanishi, T. Hayashi, O. Shimakawa, and T. Sasaki, "Spatial-spectral-efficiency-enhanced multi-core fiber," in Optical Fiber Communication Conference (OFC), Los Angeles, USA, Mar. 2015, Paper Th3C.3.

[40] K. Takenaga, Y. Arakawa, Y. Sasaki, S. Tanigawa, S. Matsuo, K. Saitoh, and M. Koshiba, "A large effective area multi-core fibre with an optimised cladding thickness," in 2011 37th European Conference and Exhibition on Optical Communication (ECOC), Geneva, Switzerland, Sep. 2011.

[41] K. Takenaga, S. Matsuo, K. Saitoh, and M. Koshiba, "Characterisation of MC fibers: New techniques and challenges," in Optical Fiber Communication Conference/National Fiber Optic Engineers Conference (OFC/NFOEC), Los Angeles, CA, USA, Mar. 2012, Paper OTu1D.5.

[42] J. Tu, K. Saitoh, M. Koshiba, K. Takenaga, and S. Matsuo, "Design and analysis of large-effective-area heterogeneous trench-assisted multi-core fiber," *Optics Express,* vol. 20, no. 14, pp. 15157-15170, Jun. 2012, doi: 10.1364/oe.20.015157.

[43] R. S. Luís, B. J. Puttnam, G. Rademacher, W. Klaus, E. Agrell, Y. Awaji, and N. Wada, "On the spectral efficiency limits of crosstalk-limited homogeneous single-mode multi-core fiber systems," in Advanced Photonics Congress (APC) New Orleans, USA, Sep. 2017, Paper NeTu2B.2.

[44] P. Bayel, C. Behrens, and D. Millar, "Modern undersea transmission technology," in *Optical Fiber Telecommunications VIB*, A. Willner, T. Li, and I. Kaminow, Academic Express, 2013.

[45] K. Kikuchi, "Fundamentals of coherent optical fiber communications," *Journal of Lightwave Technology,* vol. 34, no. 1, pp. 157 - 179, Jan. 1, 2016, doi: 10.1109/JLT.2015.2463719.

[46] B. Pinheiro, J. Rebola, and A. Cartaxo, "Impact of inter-core crosstalk on the performance of multi-core fibers-based SDM systems with coherent detection," in Proceedings of the 6th International Conference on Photonics, Optics and Laser Technology - Volume 1: PHOTOPTICS, Funchal, Madeira, Portugal, 2018.

[47] E. Ip, A. Pak, T. Lau, D. Barros, and J. Kahn, "Coherent detection in optical fiber systems," *Optics Express,* vol. 16, no. 2, pp. 753-791, Jan. 2008, doi: 10.1364/OE.16.000753.

[48] P. Bayel, C. Behrens, and D. Millar, "Commercial 100 Gbits coherent transmission systems," in *Optical Fiber Telecommunications VIB*, A. Willner, T. Li, and I. Kaminow, Academic Express, 2013.

[49] X. Liu and M. Nazarathy, "Coherent, self-coherent, and differential detection systems," in *Impact of nonlinearities on fiber optic communications*, S. Kumar, Ed., Springer, 2011.

[50] A. Carena, V. Curri, G. Bosco, P. Poggiolini, and F. Forghieri, "Modeling of the impact of nonlinear propagation effects in uncompensated optical coherent transmission links," *Journal of Lightwave Technology,* vol. 30, no. 10, pp. 1524 - 1539, May 15, 2012, doi: 10.1109/JLT.2012.2189198.

[51] R. Essiambre, G. Kramer, P. J. Winzer, G. J. Foschini, and B. Goebel, "Capacity limits of optical fiber networks," *Journal of Lightwave Technology,* vol. 28, no. 4, pp. 662-701, Feb.15, 2010, doi: 10.1109/JLT.2009.2039464.

[52] I. Tomkos, S. Azodolmolky, J. Solé-Pareta, D. Careglio, and E. Palkopoulou, "A tutorial on the flexible optical networking paradigm: State of the art, trends, and research challenges," *Proceedings of the IEEE,* vol. 102, no. 9, Sept. 2014, doi: 10.1109/JPROC.2014.2324652.

[53] O. Gerstel, M. Jinno, A. Lord, and S. Yoo, "Elastic optical networking: A new dawn for the optical layer?," *IEEE Communications Magazine,* vol. 50, no. 2, pp. s12-s20, Feb. 2012, doi: 10.1109/MCOM.2012.6146481.

[54] A. Muhammad, G. Zervas, D. Simeonidou, and R. Forchheimer, "Routing, spectrum and core allocation in flexgrid SDM networks with multi-core fibers," in 2014 International Conference on Optical Network Design and Modeling, Stockholm, Sweden, May 2014, Paper Proc. ONDM.

[55] J. Perelló, J. M. Gené, A. Pagès, J. A. Lazaro, and S. Spadaro, "Flex-grid/SDM backbone network design with inter-core XT-limited transmission reach," *IEEE/OSA Journal of Optical Communications and Networking,* vol. 8, no. 8, pp. 540 - 552, Aug. 2016, doi: 10.1364/JOCN.8.000540.

[56] *Spectral grids for WDM applications: DWDM frequency grid*, Rec. ITU-T G.694.1, International Telecommunication Union, Feb. 2012.

[57] K. Igarashi, T. Tsuritani, I. Morita, Y. Tsuchida, K. Maeda, M. Tadakuma, T. Saito, K. Watanabe, K. Imamura, R. Sugizaki, and M. Suzuki, "Super-Nyquist-WDM transmission over 7326-km seven-core fiber with capacity-distance product of 1.03 Exabit/s·km," *Optics Express,* vol. 22, no. 2, pp. 1220-1228, Jan. 2014, doi: 10.1364/OE.22.001220.

[58] T. Hayashi and T. Sasaki, "Design strategy of uncoupled multicore fiber enabling high spatial capacity transmission," in 2013 IEEE Photonics Society Summer Topical Meeting Series, Waikoloa, HI, July 2013, Paper MC2.4.

[59] E. Specht, "Packings of equal and unequal circles in fixed-sized containers with maximum packing density", Available: http://www.packomania.com/

[60] F. Ye, J. Tu, K. Saitoh, and T. Morioka, "Simple analytical expression for crosstalk estimation in homogeneous trench-assisted multi-core fibers," *Optics Express,* vol. 22, no. 19, pp. 23007-23018, Sep. 2014, doi: 10.1364/oe.22.023007.

[61] P. Bayvel, C. Behrens, and D. Millar, "Digital signal processing (DSP) and its application in optical communication systems," in *Optical Fiber Telecommunications VIB*, A. Willner, T. Li, and I. Kaminow, Academic Express, 2013.

[62] B. J. Puttnam, R. S. Luís, T. A. Eriksson, W. Klaus, J.-M. Delgado Mendinueta, Y. Awaji and N. Wada, "Impact of intercore crosstalk on the transmission distance of QAM formats in multicore fibers, " *IEEE Photonics Journal,* vol 8, no. 2, p 1-9, April 2016, doi:10.1109/JPHOT.2016.2523993.

[63] F. Ye, J. Tu, K. Saitoh, K. Takenaga, S. Matsuo, H. Takara, and T. Morioka, "Wavelength-dependence of inter-core crosstalk in homogeneous multi-core fibers," *IEEE Photonics Technology Letters,* vol. 28, no. 1, pp. 27-30, Jan 1. 2016, doi: 10.1109/LPT.2015.2478911.

[64] P. Poggiolini, "Analytical modeling of non-linear propagation in coherent systems," in 2012 38th European Conference and Exhibition on Optical Communications (ECOC), Amsterdam, Netherlands, Sept. 2012.

[65] K. Okamoto, "Optical Fibers," in *Fundamentals of Optical Waveguides* A. Press, Ed. 2nd ed., 2006, p. 71.

Appendix A. – Coupling coefficient approximation

For large arguments of $(a+b)x$, the modified Bessel function of the first kind can be approximated as [60]:

$$I_0[(a+b)x] \approx \frac{1}{\sqrt{2\pi(a+b)x}} \exp[(a+b)x] \tag{A.1}$$

Where $a>b>0$. If b is relatively small compared to a, the modified Bessel function of the first kind $I_0[(a+b)x]$ can be related to $I_0(ax)$ by the following expression

$$I_0[(a+b)x] \approx \sqrt{\frac{a}{a+b}} I_0(ax)\exp(bx) \tag{A.2}$$

Typical values of $\Lambda_{m,n}$ (around 30 μm) can be more than 5 times larger than the typical trench width (around 4.5 μm), thus $(P_1-P_2+Y_1-Y_2)/(\Lambda_{m,n}-r) = (W_2-W_1)w_{tr}/[a_1(\Lambda_{m,n}-r)] > 0$ is much smaller than W_1/a_1. Considering Equation (A.2), the expression $I_0\left[\left(\frac{W_1}{a_1}+\frac{P_1-P_2+Y_1-Y_2}{\Lambda_{m,n}-r}\right)r\right]$ can be written as [60]:

$$I_0\left[\left(\frac{W_1}{a_1}+\frac{P_1-P_2+Y_1-Y_2}{\Lambda_{m,n}-r}\right)r\right] \approx \sqrt{\Gamma} I_0\left(\frac{W_1}{a_1}r\right)\exp\left(\frac{P_1-P_2+Y_1-Y_2}{\Lambda_{m,n}-r}\right) \tag{A.3}$$

Since $(P_1-P_2+Y_1-Y_2)/(\Lambda_{m,n}-r)$ is much smaller than W_1/a_1 and r is much smaller than $\Lambda_{m,n}$, the dependence on the parameter r can be eliminated and the parameter Γ can be simplified to

$$\Gamma = \frac{W_1/a_1}{W_1/a_1+(P_1-P_2+Y_1-Y_2)/\Lambda_{m,n}} = \frac{W_1}{W_1+(W_2-W_1)w_{tr}/\Lambda_{m,n}} \tag{A.4}$$

The mode coupling coefficient for a step index structure can be expressed as [60] :

$$k_{mn}^{'} = k(n_1^2 - n_0^2)\frac{W_1^2}{n_1 a_1^2 V_1^2 J_1^2(U_1)}\frac{J_0(U_1)}{K_0(W_1)}\sqrt{\frac{\pi a_1}{2W_1\Lambda_{m,n}}}\exp\left(-\frac{W_1}{a_1}\Lambda_{m,n}\right)\int_0^{a_1} J_0\left(\frac{U_1}{a_1}r\right)I_0\left(\frac{W_1}{a_1}r\right)rdr \tag{A.5}$$

Comparing Equation (A.5) with Equation (3.8), the ratio between the two structures is given by

$$\frac{k_{mn}}{k_{mn}^{'}} = \frac{U_1 L_q \int_0^{a_1} J_0\left(\frac{U_1}{a_1}r\right)I_0\left[\left(\frac{W_1}{a_1} + \frac{P_1 - P_2 + Y_1 - Y_2}{\Lambda_{m,n} - r}\right)r\right]\exp\left(-\frac{P_1 - P_2 + Y_1 - Y_2}{\Lambda_{m,n} - r}\Lambda_{m,n}\right)rdr}{W_1\frac{J_0(U_1)}{K_0(W_1)}\int_0^{a_1} J_0\left(\frac{U_1}{a_1}r\right)I_0\left(\frac{W_1}{a_1}r\right)rdr} \tag{A.6}$$

Substituting Equation (A.3) into Equation (A.6), the ratio between the mode coupling coefficients for the two structures is given by [60]

$$\frac{k_{mn}}{k_{mn}^{'}} = \frac{U_1 L_q \int_0^{a_1} J_0\left(\frac{U_1}{a_1}r\right)\sqrt{\Gamma}I_0\left(\frac{W_1}{a_1}r\right)\exp\left(\frac{P_1 - P_2 + Y_1 - Y_2}{\Lambda_{m,n} - r}r\right)\exp\left(-\frac{P_1 - P_2 + Y_1 - Y_2}{\Lambda_{m,n} - r}\Lambda_{m,n}\right)rdr}{W_1\frac{J_0(U_1)}{K_0(W_1)}\int_0^{a_1} J_0\left(\frac{U_1}{a_1}r\right)I_0\left(\frac{W_1}{a_1}r\right)rdr} \tag{A.7}$$

Solving Equation (A.7) the ratio between the mode coupling coefficients for the two structures becomes [60]:

$$\frac{k_{mn}}{k_{mn}^{'}} = \frac{\sqrt{\Gamma}U_1 L_q \exp\left[-(P_1 - P_2 + Y_1 - Y_2)\right]}{W_1\frac{J_0(U_1)}{K_0(W_1)}} \tag{A.8}$$

Assuming n=1 in the dispersion Equation (3.71) in [65] for step index fiber, then [60]

$$\frac{J_0(U_1)}{U_1 J_1(U_1)} = \frac{K_0(W_1)}{W_1 K_1(W_1)} \tag{A.9}$$

Substituting Equation (A.9) into Equation (A.8) the ratio between the two structures is simplified to

$$\frac{k_{mn}}{k_{mn}^{'}} = \frac{\sqrt{\Gamma}L_q \exp\left[-(P_1 - P_2 + Y_1 - Y_2)\right]}{\frac{J_1(U_1)}{K_1(W_1)}} \tag{A.10}$$

For $x \geq 2$, the modified Bessel function of the second kind can be approximated as [60]

$$K_1(x) \approx K_0(x) \approx \sqrt{\frac{\pi}{2x}} \exp(-x) \tag{A.11}$$

So, the parameter L_q can be simplified to

$$L_q = \frac{J_1(U_1)}{K_1(W_1)} \exp\left[-(W_2 - W_1) \frac{w_{tr}}{a_1} \right] \tag{A.12}$$

The ratio between the mode coupling coefficient for the two structures becomes

$$\frac{k_{mn}}{k_{mn}^{'}} = \sqrt{\Gamma} \exp\left[-(P_1 - P_2 + Y_1 - Y_2) \right] \exp\left[-(W_2 - W_1) \frac{w_{tr}}{a_1} \right] = \sqrt{\Gamma} \exp\left[-2(W_2 - W_1) \frac{w_{tr}}{a_1} \right] \tag{A.13}$$

The mode coupling coefficient for a step index structure can be simplified as [60]

$$k_{mn}^{'} = \frac{\sqrt{\Delta_1}}{a_1} \frac{U_1^2}{V_1^3 K_1^2(W_1)} \sqrt{\frac{\pi a_1}{W_1 \Lambda_{m,n}}} \exp\left(-\frac{W_1}{a_1} \Lambda_{m,n} \right) \tag{A.14}$$

Replacing $k_{mn}^{'}$ given by Equation (A.14) into the ratio given by Equation (A.13), the mode coupling coefficient k_{mn} between two neighbouring cores with trench-assisted structures can be expressed as [60]

$$k_{mn} \simeq \frac{\sqrt{\Gamma}\sqrt{\Delta_1}}{a_1} \frac{U_1^2}{V_1^3 K_1^2(W_1)} \sqrt{\frac{\pi a_1}{W_1 \Lambda_{m,n}}} \exp\left[-\frac{W_1 \Lambda + 2(W_2 - W_1) w_{tr}}{a_1} \right] \tag{A.15}$$

Appendix B. – Nominal central frequencies for each modulation format

The nominal central frequencies considered in this work for the 4-QAM modulation format for each channel of the 80 WDM channels each with 50 GHz channel width are represented in Table B.1.

Table B.1- Nominal central frequencies for each channel for 4-QAM.

Number of channel	Central frequency	Units	Number of channel	Central frequency	Units
1	191.75	THz	**41**	193.75	THz
2	191.8	THz	**42**	193.8	THz
3	191.85	THz	**43**	193.85	THz
4	191.9	THz	**44**	193.9	THz
5	191.95	THz	**45**	193.95	THz
6	192	THz	**46**	194	THz
7	192.05	THz	**47**	194.05	THz
8	192.1	THz	**48**	194.1	THz
9	192.15	THz	**49**	194.15	THz
10	192.2	THz	**50**	194.2	THz
11	192.25	THz	**51**	194.25	THz
12	192.3	THz	**52**	194.3	THz
13	192.35	THz	**53**	194.35	THz
14	192.4	THz	**54**	194.4	THz
15	192.45	THz	**55**	194.45	THz
16	192.5	THz	**56**	194.5	THz
17	192.55	THz	**57**	194.55	THz
18	192.6	THz	**58**	194.6	THz
19	192.65	THz	**59**	194.65	THz
20	192.7	THz	**60**	194.7	THz
21	192.75	THz	**61**	194.75	THz
22	192.8	THz	**62**	194.8	THz
23	192.85	THz	**63**	194.85	THz
24	192.9	THz	**64**	194.9	THz
25	192.95	THz	**65**	194.95	THz
26	193	THz	**66**	195	THz
27	193.05	THz	**67**	195.05	THz
28	193.1	THz	**68**	195.1	THz
29	193.15	THz	**69**	195.15	THz
30	193.2	THz	**70**	195.2	THz
31	193.25	THz	**71**	195.25	THz
32	193.3	THz	**72**	195.3	THz
33	193.35	THz	**73**	195.35	THz

34	193.4	THz	**74**	195.4	THz
35	193.45	THz	**75**	195.45	THz
36	193.5	THz	**76**	195.5	THz
37	193.55	THz	**77**	195.55	THz
38	193.6	THz	**78**	195.6	THz
39	193.65	THz	**79**	195.65	THz
40	193.7	THz	**80**	195.7	THz

The nominal central frequencies considered in this work for 8-QAM and 16-QAM modulation formats for each channel of the 106 WDM channels each with 37.5 GHz channel width are represented in Table B.2.

Table B.2 – Nominal central frequencies for each channel for 8-QAM and 16-QAM

Number of channel	Central frequency	Units	Number of channel	Central frequency	Units
1	191.7875	THz	**54**	193.775	THz
2	191.825	THz	**55**	193.8125	THz
3	191.8625	THz	**56**	193.85	THz
4	191.9	THz	**57**	193.8875	THz
5	191.9375	THz	**58**	193.925	THz
6	191.975	THz	**59**	193.9625	THz
7	192.0125	THz	**60**	194	THz
8	192.05	THz	**61**	194.0375	THz
9	192.0875	THz	**62**	194.075	THz
10	192.125	THz	**63**	194.1125	THz
11	192.1625	THz	**64**	194.15	THz
12	192.2	THz	**65**	194.1875	THz
13	192.2375	THz	**66**	194.225	THz
14	192.275	THz	**67**	194.2625	THz
15	192.3125	THz	**68**	194.3	THz
16	192.35	THz	**69**	194.3375	THz
17	192.3875	THz	**70**	194.375	THz
18	192.425	THz	**71**	194.4125	THz
19	192.4625	THz	**72**	194.45	THz
20	192.5	THz	**73**	194.4875	THz
21	192.5375	THz	**74**	194.525	THz
22	192.575	THz	**75**	194.5625	THz
23	192.6125	THz	**76**	194.6	THz
24	192.65	THz	**77**	194.6375	THz
25	192.6875	THz	**78**	194.675	THz
26	192.725	THz	**79**	194.7125	THz
27	192.7625	THz	**80**	194.75	THz
28	192.8	THz	**81**	194.7875	THz
29	192.8375	THz	**82**	194.825	THz
30	192.875	THz	**83**	194.8625	THz
31	192.9125	THz	**84**	194.9	THz
32	192.95	THz	**85**	194.9375	THz

33	192.9875	THz	**86**	194.975	THz
34	193.025	THz	**87**	195.0125	THz
35	193.0625	THz	**88**	195.05	THz
36	193.1	THz	**89**	195.0875	THz
37	193.1375	THz	**90**	195.125	THz
38	193.175	THz	**91**	195.1625	THz
39	193.2125	THz	**92**	195.2	THz
40	193.25	THz	**93**	195.2375	THz
41	193.2875	THz	**94**	195.275	THz
42	193.325	THz	**95**	195.3125	THz
43	193.3625	THz	**96**	195.35	THz
44	193.4	THz	**97**	195.3875	THz
45	193.4375	THz	**98**	195.425	THz
46	193.475	THz	**99**	195.4625	THz
47	193.5125	THz	**100**	195.5	THz
48	193.55	THz	**101**	195.5375	THz
49	193.5875	THz	**102**	195.575	THz
50	193.625	THz	**103**	195.6125	THz
51	193.6625	THz	**104**	195.65	THz
52	193.7	THz	**105**	195.6875	THz
53	193.7375	THz	**106**	195.725	THz

The nominal central frequencies considered in this work for 32-QAM and 64-QAM modulation formats for each channel of the 160 WDM channels each width 25 GHz channel width are represented in Table B.3.

Table B.3- Nominal central frequencies for each channel for 32-QAM and 64-QAM

Number of channel	Central frequency	Units	Number of channel	Central frequency	Units
1	191.725	THz	**81**	193.725	THz
2	191.75	THz	**82**	193.75	THz
3	191.775	THz	**83**	193.775	THz
4	191.8	THz	**84**	193.8	THz
5	191.825	THz	**85**	193.825	THz
6	191.85	THz	**86**	193.85	THz
7	191.875	THz	**87**	193.875	THz
8	191.9	THz	**88**	193.9	THz
9	191.925	THz	**89**	193.925	THz
10	191.95	THz	**90**	193.95	THz
11	191.975	THz	**91**	193.975	THz
12	192	THz	**92**	194	THz
13	192.025	THz	**93**	194.025	THz
14	192.05	THz	**94**	194.05	THz
15	192.075	THz	**95**	194.075	THz
16	192.1	THz	**96**	194.1	THz
17	192.125	THz	**97**	194.125	THz
18	192.15	THz	**98**	194.15	THz
19	192.175	THz	**99**	194.175	THz

20	192.2	THz	**100**	194.2	THz
21	192.225	THz	**101**	194.225	THz
22	192.25	THz	**102**	194.25	THz
23	192.275	THz	**103**	194.275	THz
24	192.3	THz	**104**	194.3	THz
25	192.325	THz	**105**	194.325	THz
26	192.35	THz	**106**	194.35	THz
27	192.375	THz	**107**	194.375	THz
28	192.4	THz	**108**	194.4	THz
29	192.425	THz	**109**	194.425	THz
30	192.45	THz	**110**	194.45	THz
31	192.475	THz	**111**	194.475	THz
32	192.5	THz	**112**	194.5	THz
33	192.525	THz	**113**	194.525	THz
34	192.55	THz	**114**	194.55	THz
35	192.575	THz	**115**	194.575	THz
36	192.6	THz	**116**	194.6	THz
37	192.625	THz	**117**	194.625	THz
38	192.65	THz	**118**	194.65	THz
39	192.675	THz	**119**	194.675	THz
40	192.7	THz	**120**	194.7	THz
41	192.725	THz	**121**	194.725	THz
42	192.75	THz	**122**	194.75	THz
43	192.775	THz	**123**	194.775	THz
44	192.8	THz	**124**	194.8	THz
45	192.825	THz	**125**	194.825	THz
46	192.85	THz	**126**	194.85	THz
47	192.875	THz	**127**	194.875	THz
48	192.9	THz	**128**	194.9	THz
49	192.925	THz	**129**	194.925	THz
50	192.95	THz	**130**	194.95	THz
51	192.975	THz	**131**	194.975	THz
52	193	THz	**132**	195	THz
53	193.025	THz	**133**	195.025	THz
54	193.05	THz	**134**	195.05	THz
55	193.075	THz	**135**	195.075	THz
56	193.1	THz	**136**	195.1	THz
57	193.125	THz	**137**	195.125	THz
58	193.15	THz	**138**	195.15	THz
59	193.175	THz	**139**	195.175	THz
60	193.2	THz	**140**	195.2	THz
61	193.225	THz	**141**	195.225	THz
62	193.25	THz	**142**	195.25	THz
63	193.275	THz	**143**	195.275	THz
64	193.3	THz	**144**	195.3	THz
65	193.325	THz	**145**	195.325	THz
66	193.35	THz	**146**	195.35	THz
67	193.375	THz	**147**	195.375	THz
68	193.4	THz	**148**	195.4	THz
69	193.425	THz	**149**	195.425	THz

70	193.45	THz	**150**	195.45	THz
71	193.475	THz	**151**	195.475	THz
72	193.5	THz	**152**	195.5	THz
73	193.525	THz	**153**	195.525	THz
74	193.55	THz	**154**	195.55	THz
75	193.575	THz	**155**	195.575	THz
76	193.6	THz	**156**	195.6	THz
77	193.625	THz	**157**	195.625	THz
78	193.65	THz	**158**	195.65	THz
79	193.675	THz	**159**	195.675	THz
80	193.7	THz	**160**	195.7	THz